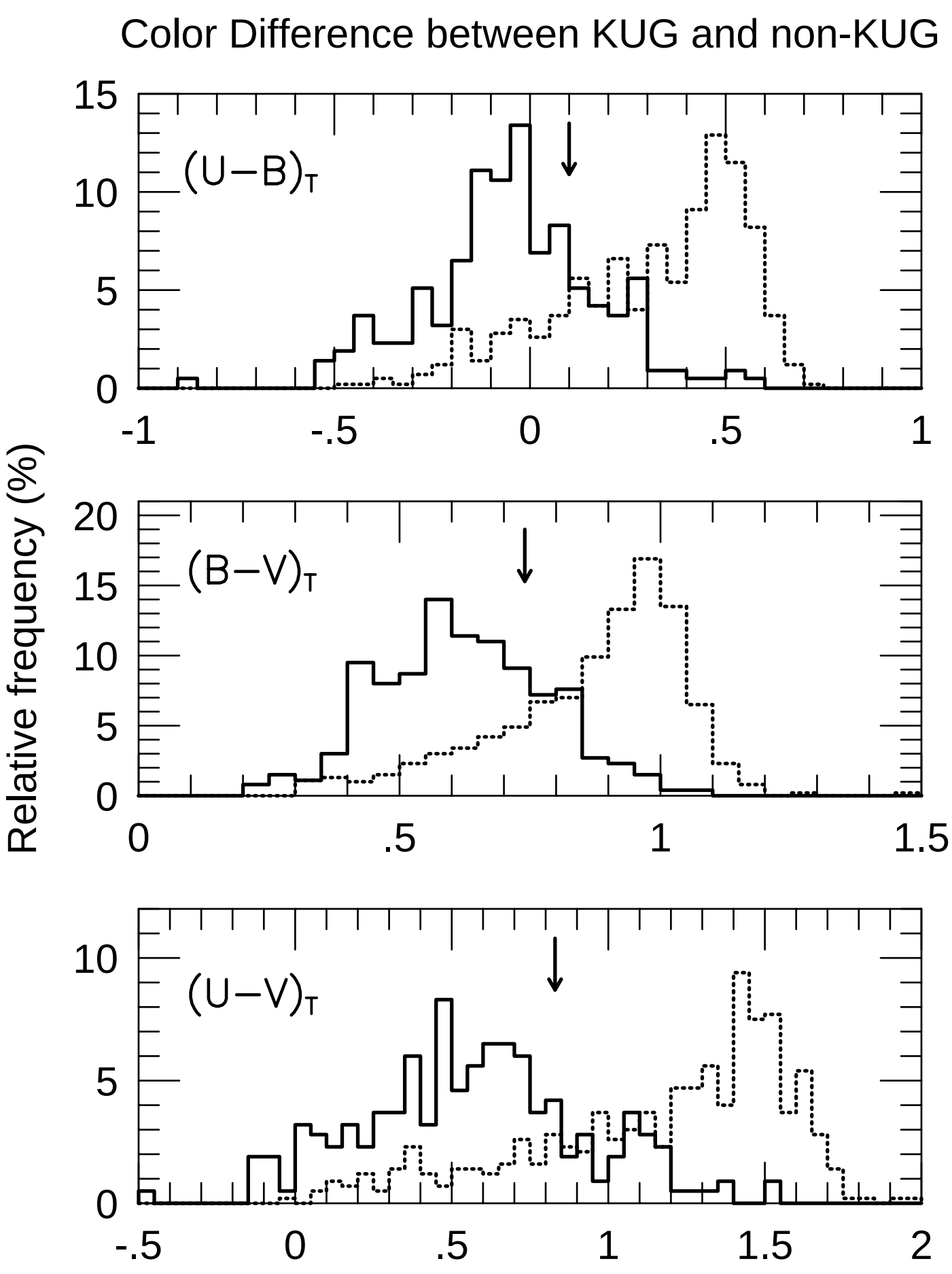
Color Difference between KUG and non-KUG
Relative frequency (%)
(U−B)T
(B−V)T
(U−V)T
15
10
5
0
-1
-.5
0
.5
1
20
15
10
5
0
0
.5
1
1.5
10
5
0
-.5
0
.5
1
1.5
2

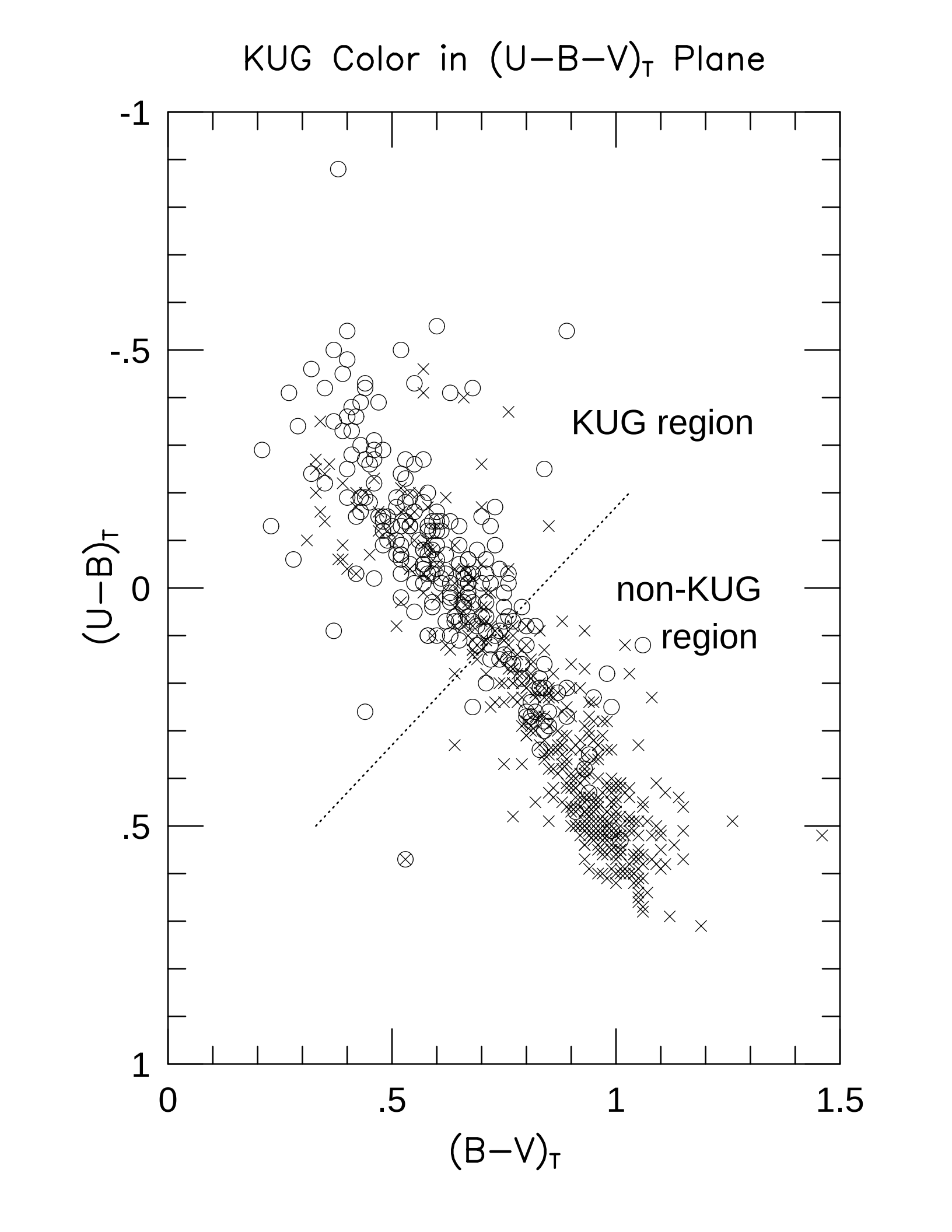
KUG Color in $(U-B-V)_T$ Plane
KUG region
non-KUG region
$(U-B)_T$
$(B-V)_T$
-1
-.5
0
.5
1
0
.5
1
1.5

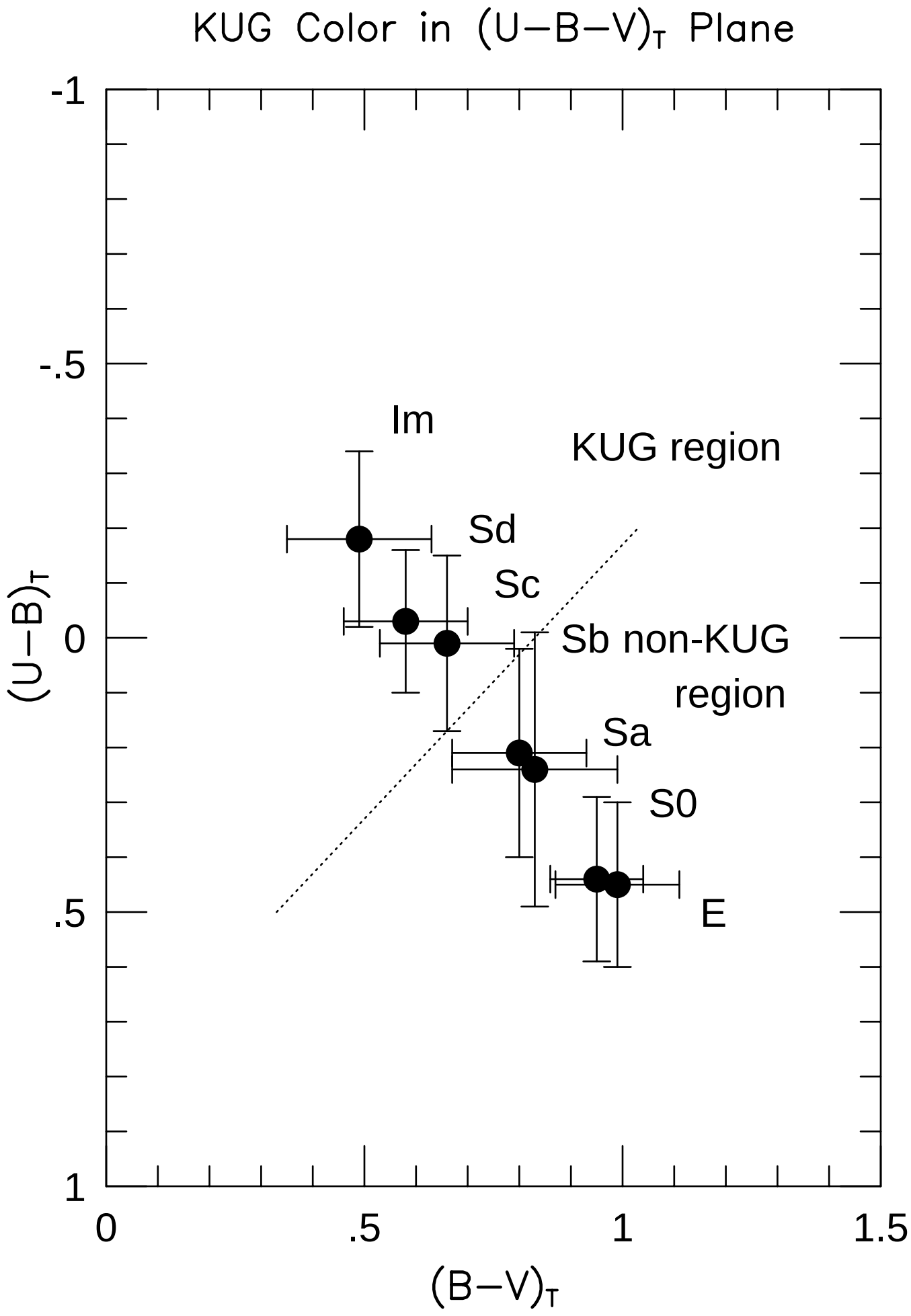
KUG Color in $(U-B-V)_T$ Plane
-1
-.5
0
.5
1
0
.5
1
1.5
$(U-B)_T$
$(B-V)_T$
Im
Sd
Sc
Sb
Sa
S0
E
KUG region
non-KUG region

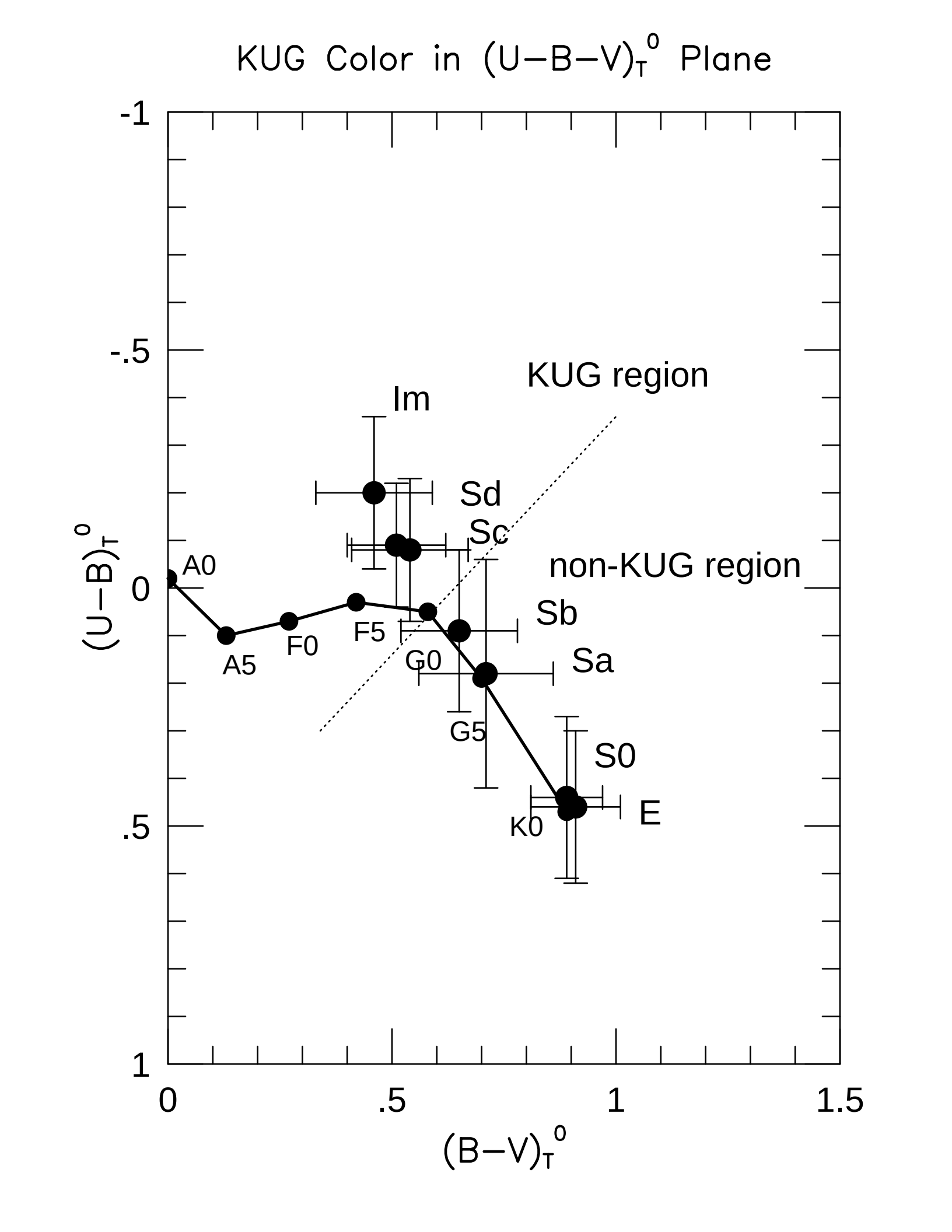
KUG Color in $(U-B-V)_T^0$ Plane
-1
-.5
0
.5
1
0
.5
1
1.5
$(U-B)_T^0$
$(B-V)_T^0$
KUG region
non-KUG region
Im
Sd
Sc
Sb
Sa
S0
E
A0
A5
F0
F5
G0
G5
K0

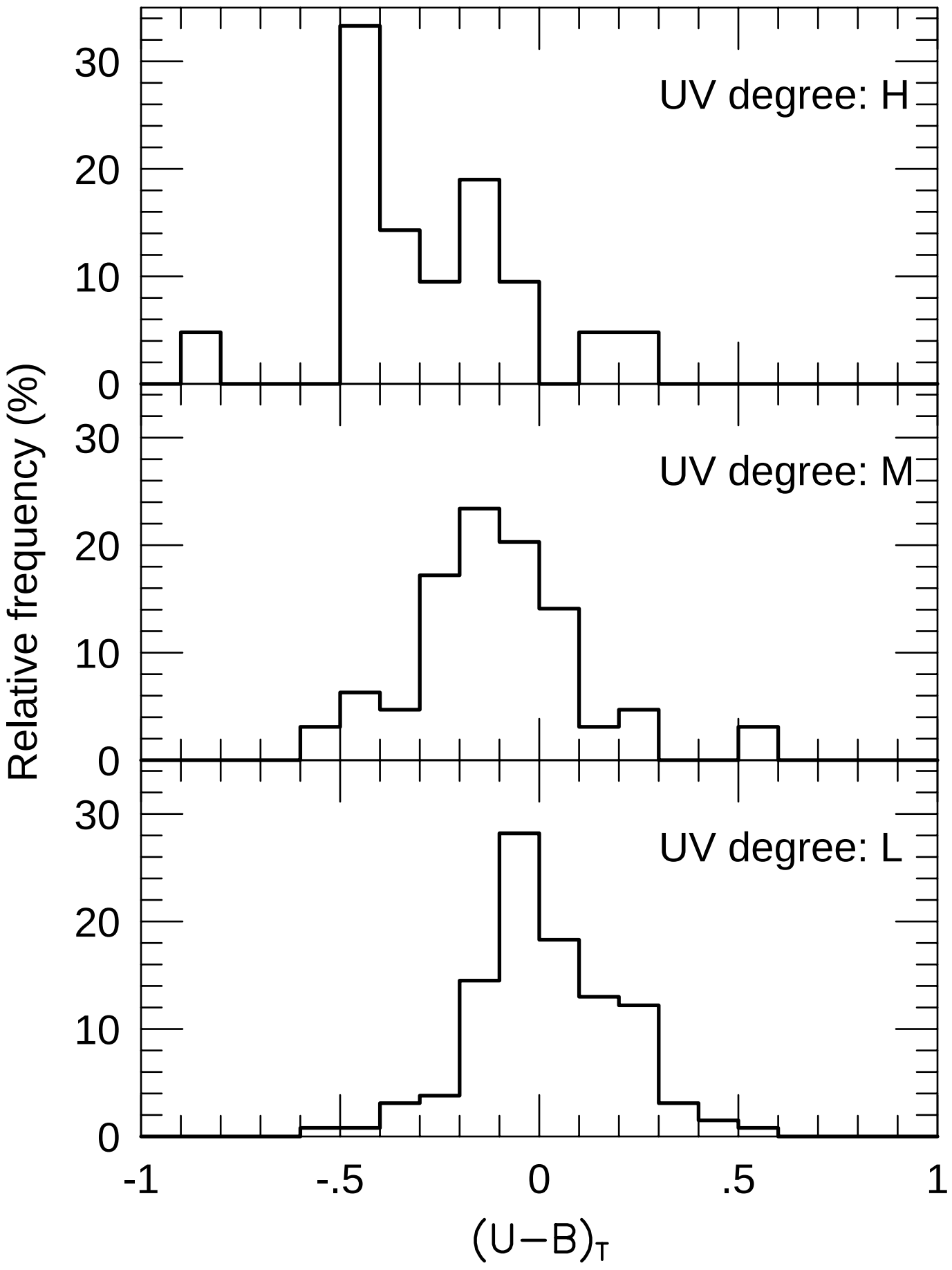
Color Difference along the UV Degree
UV degree: H
UV degree: M
UV degree: L
Relative frequency (%)
30
20
10
0
-1
-.5
0
.5
1
(U−B)T

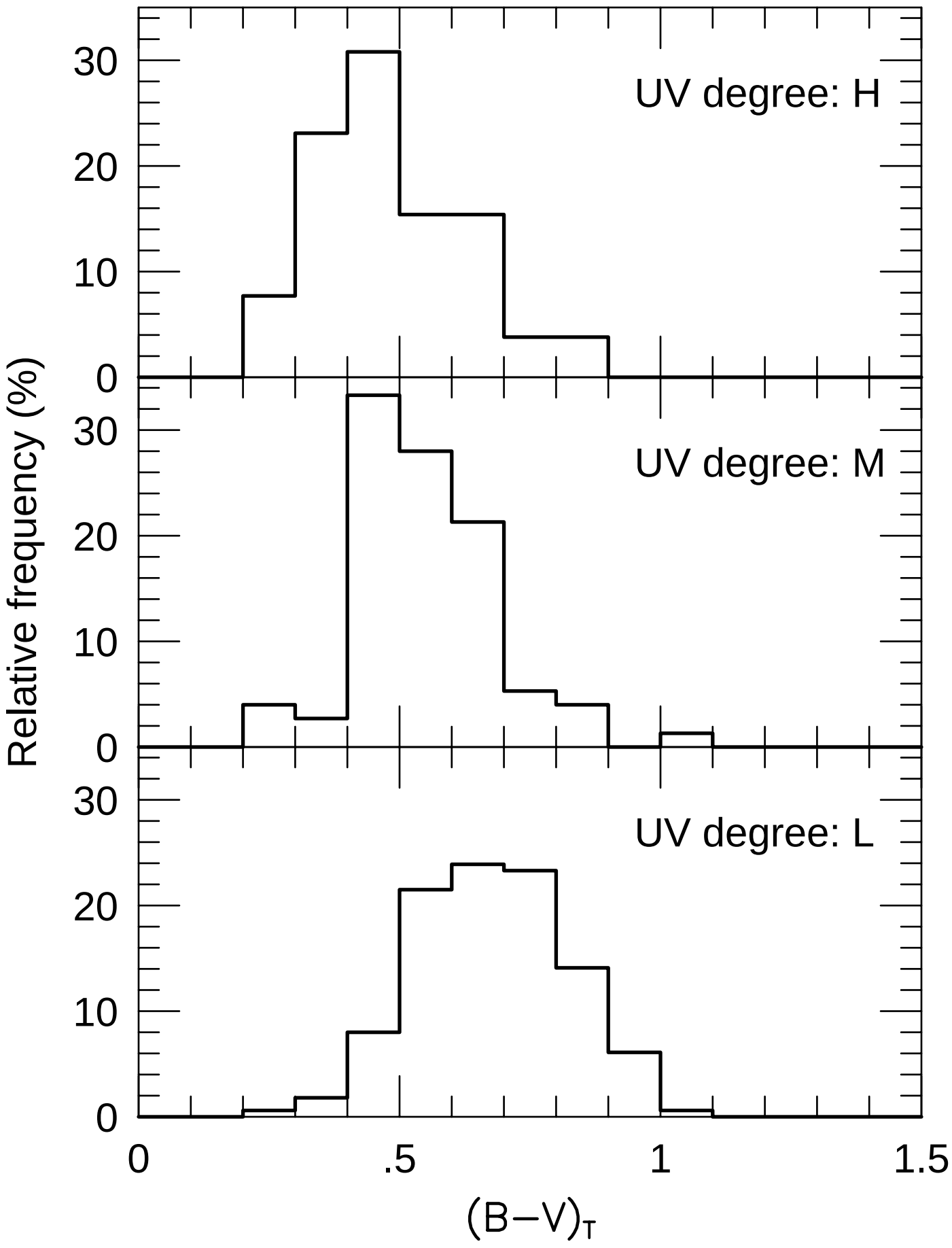
Color Difference along the UV Degree
UV degree: H
UV degree: M
UV degree: L
Relative frequency (%)
0
10
20
30
0
.5
1
1.5
(B−V)T

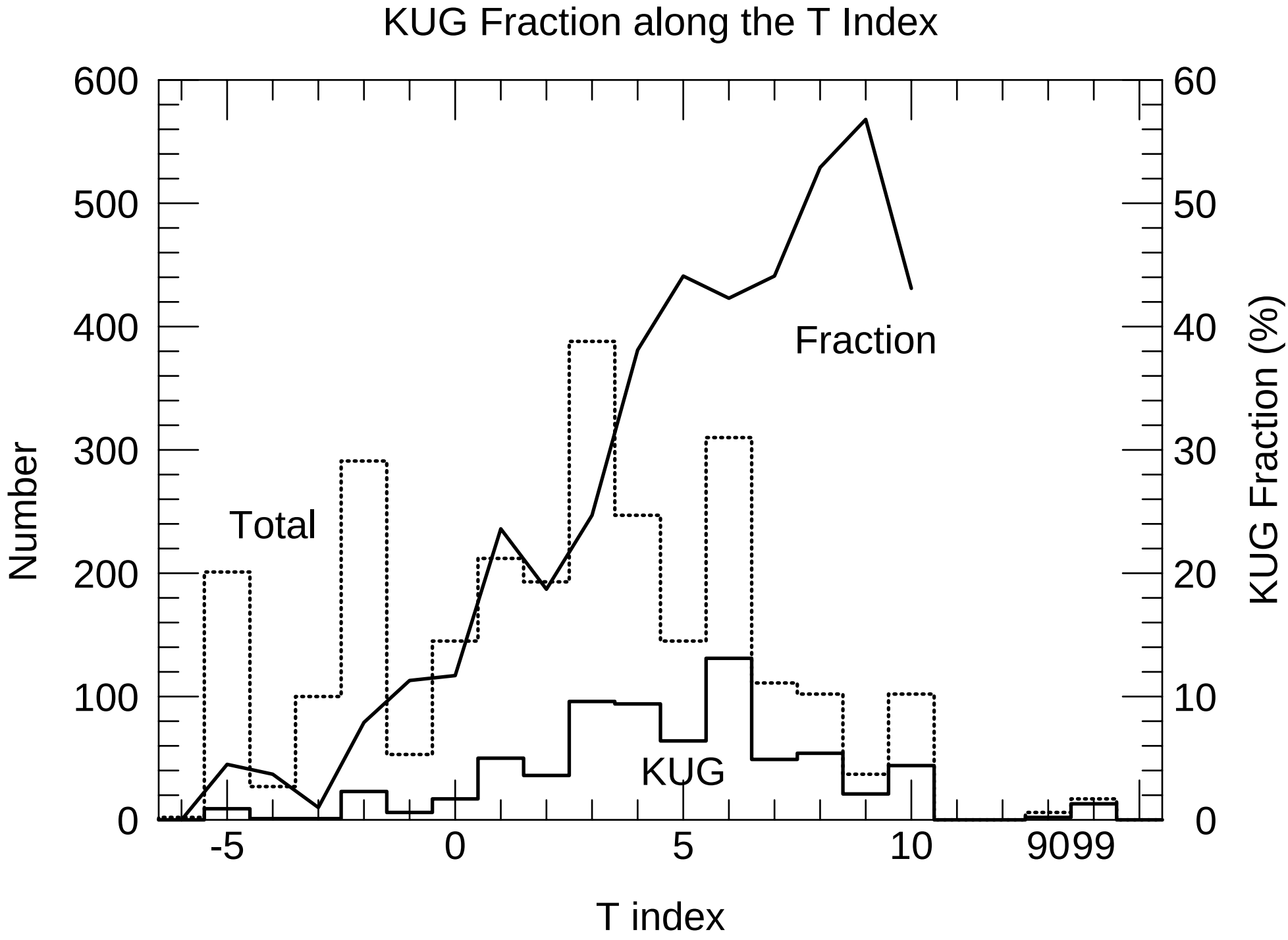
KUG Fraction along the T Index
600
500
400
300
200
100
0
60
50
40
30
20
10
0
Number
KUG Fraction (%)
Total
Fraction
KUG
-5
0
5
10
9099
T index

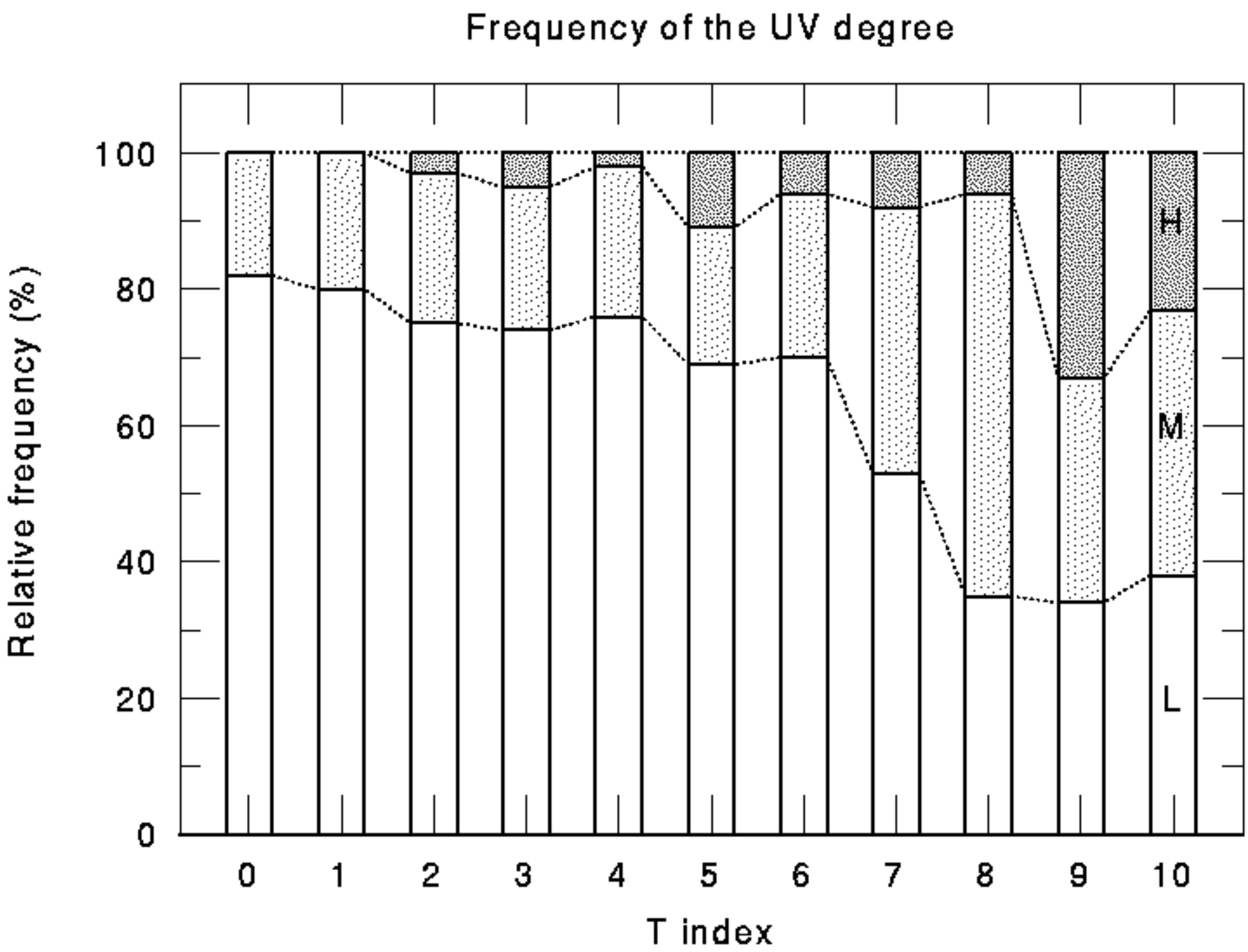
Frequency of the UV degree
Relative frequency (%)
100
80
60
40
20
0
0
1
2
3
4
5
6
7
8
9
10
T index
H
M
L

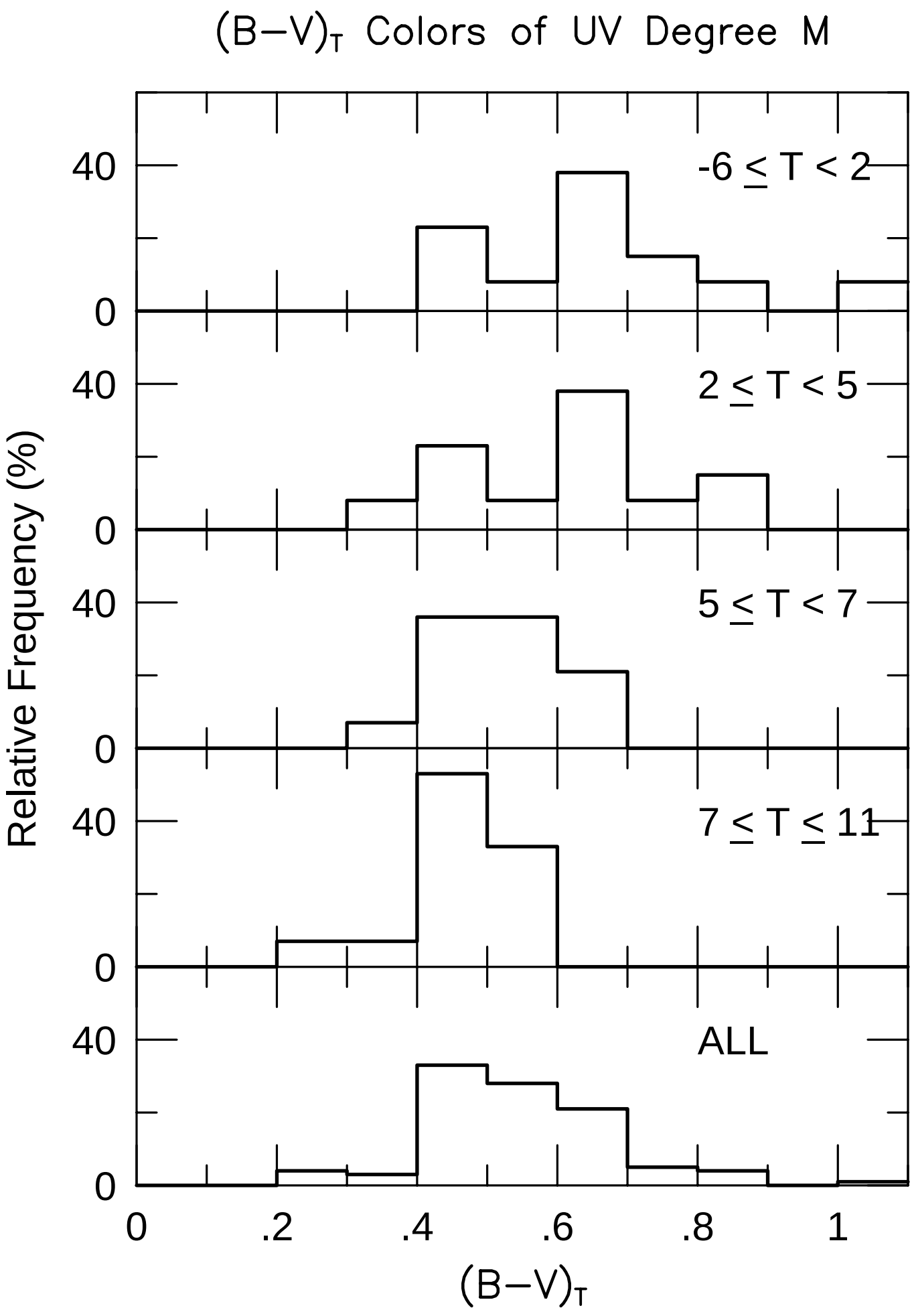
(B−V)T Colors of UV Degree M
-6 ≤ T < 2
2 ≤ T < 5
5 ≤ T < 7
7 ≤ T ≤ 11
ALL
40
0
Relative Frequency (%)
0
.2
.4
.6
.8
1
(B−V)T

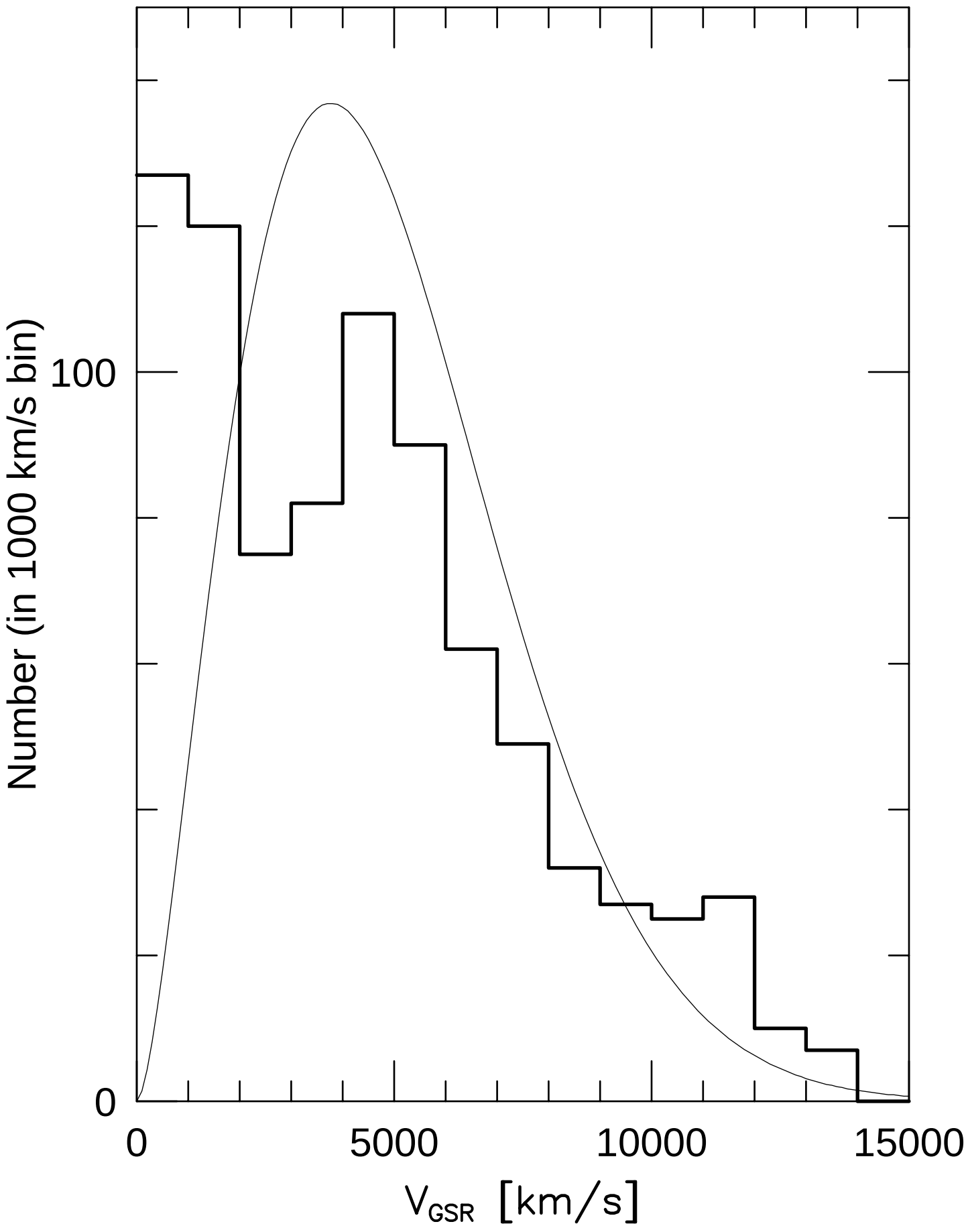
Radial Velocity Distribution of the Total Sample
Number (in 1000 km/s bin)
100
0
0
5000
10000
15000
V_{GSR} [km/s]

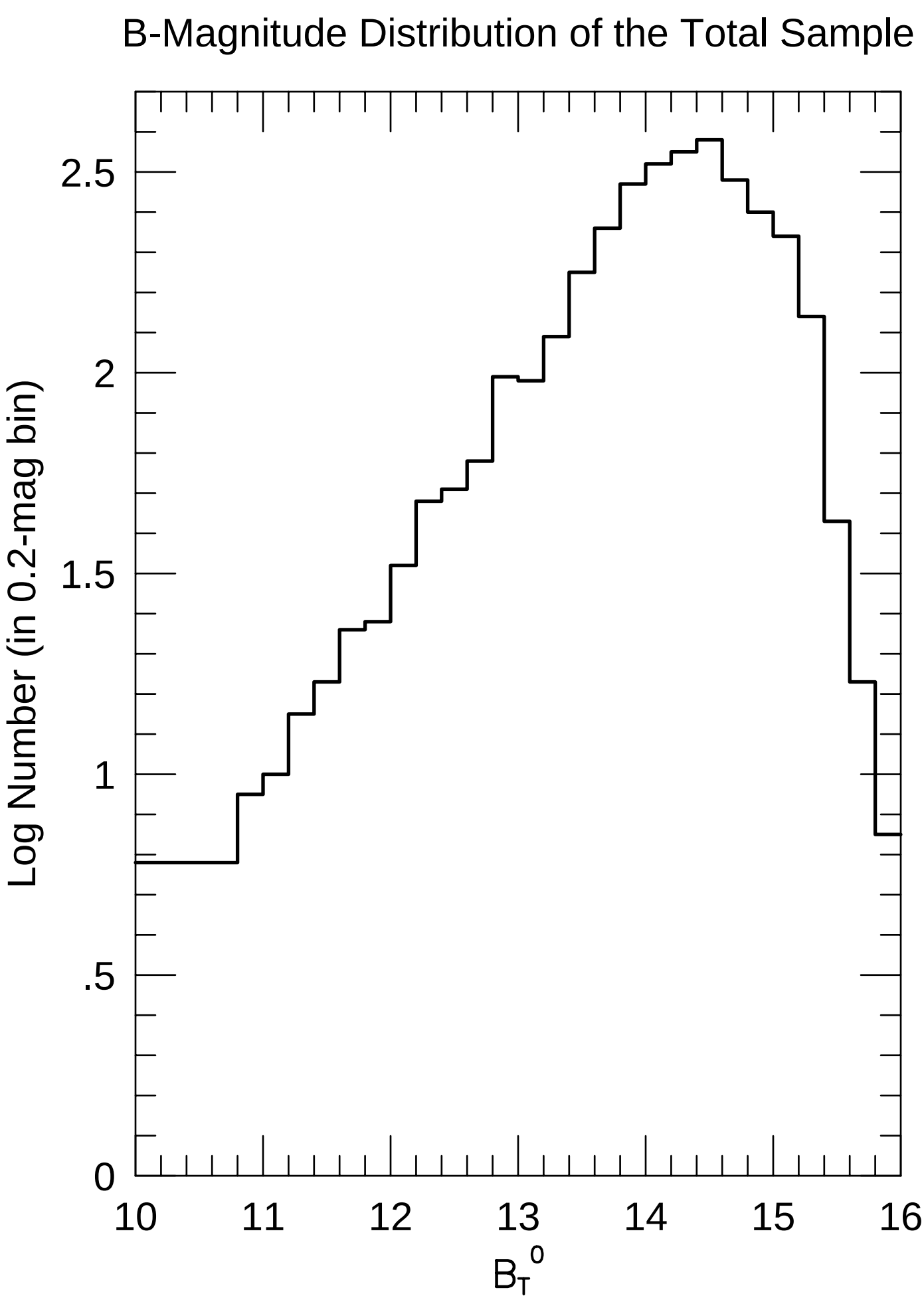
B-Magnitude Distribution of the Total Sample
Log Number (in 0.2-mag bin)
2.5
2
1.5
1
.5
0
10
11
12
13
14
15
16
B_T^0

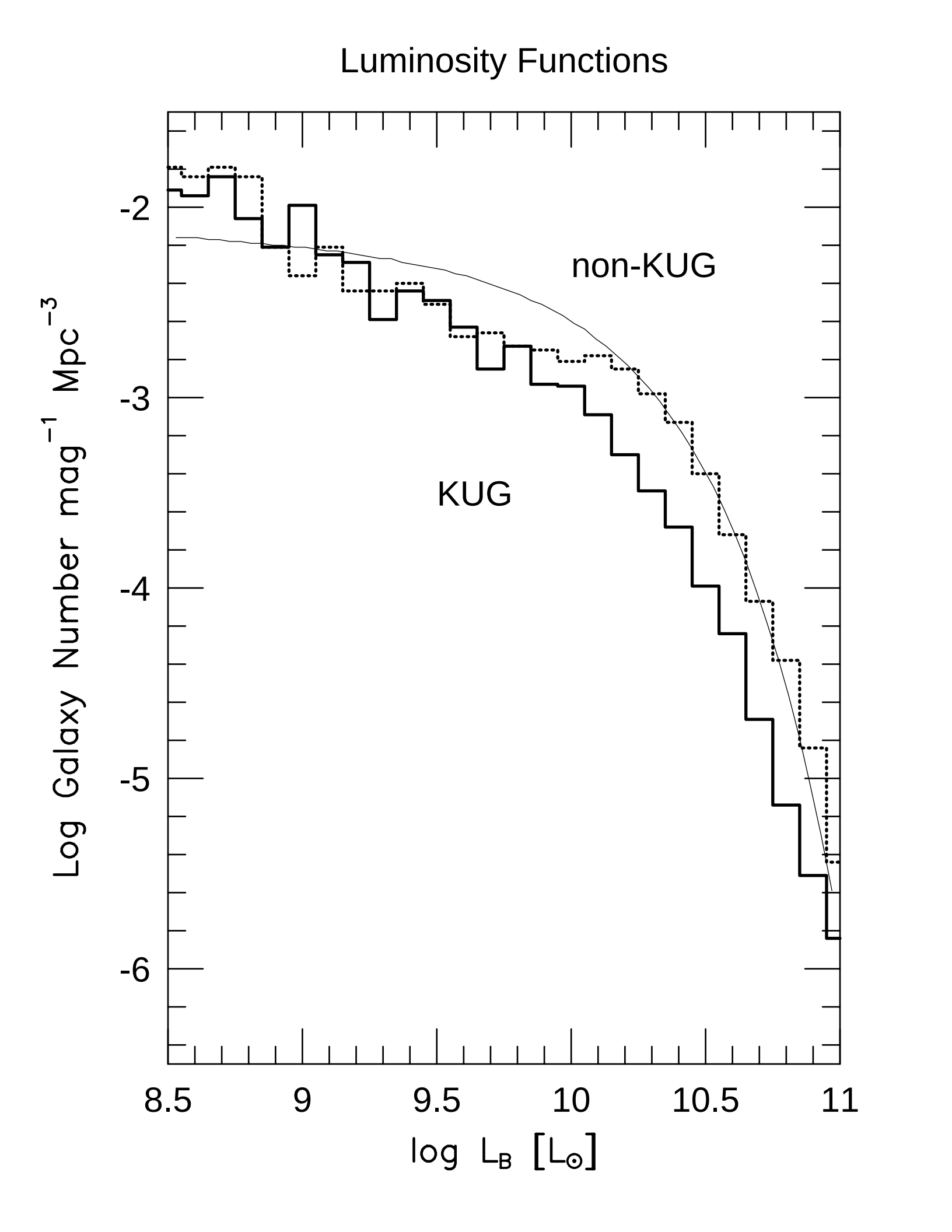
Luminosity Functions
non-KUG
KUG
-2
-3
-4
-5
-6
8.5
9
9.5
10
10.5
11
Log Galaxy Number mag^{-1} Mpc^{-3}
log L_B [$L_\odot$]

Characteristics of Kiso Ultra-Violet Excess Galaxies

Akihiko Tomita

Department of Earth and Astronomical Sciences,

Faculty of Education, Wakayama University,

930 Sakae-Dani, Wakayama 640, Japan

Electronic mail: atomita@center.wakayama-u.ac.jp

and

Tsutomu T. Takeuchi[1], Tadashi Usui, and Mamoru Saitō

Department of Astronomy, Faculty of Science, Kyoto University,

Sakyo-ku, Kyoto 606-01, Japan

Electronic mail: takeuchi, usui, saitom@kusastro.kyoto-u.ac.jp

Received 11 June 1997; accepted 6 August 1997

To be appeared in The Astronomical Journal, Vol. 114, No. 5 (1997 Nov issue)

[1] Research Fellow of the Japan Society for the Promotion of Science

ABSTRACT

We examined the general characteristics of the Kiso Ultra-violet Excess Galaxies (KUGs). We present for the first time the quantitative expressions for the criteria of the KUGs; the boundary color separating the KUGs from the non-KUGs is $(B-V)_{\rm T}=0.74$ and the KUG degrees of UV strength are found to correlate with the mean $(B-V)_{\rm T}$ colors. We investigate the nature of the KUGs, a sample of blue galaxy population, and show that (1) about a half of the KUGs are spiral galaxies with Sb to Scd, (2) the KUGs are biased to late-type galaxies and include early-type galaxies with young star populations, and (3) the KUGs are preferably found among less luminous galaxies with $L_B < 10^{10} L_{\odot}$. The KUGs also contain the post-starburst galaxies, many of which are found among the blue galaxy population at intermediate redshifts. The analysis of the far-infrared data shows that a typical present-to-past star formation rate for a KUG is 0.4.

Subject headings: galaxies: KUG, star formation, post-starburst, blue galaxy population

1. Introduction

Kiso Ultraviolet-Excess Galaxies (hereafter KUGs) are a UV-excess galaxy sample surveyed by means of the plates taken by the Kiso Observatory 1.05-m Schmidt telescope, the compiled catalog of which was given by Takase, Miyauchi-Isobe (1993) (TM93). KUGs were selected by eye-inspection among galaxies on the Schmidt plates made by the U, G, R three-image method if the objects had U-images brighter than G and R-images; the exposure times were so adjusted that an A0 star would have an equal brightness for the three images. The survey method, however, did not introduce quantitative criteria of the KUGs.

Many follow-up observations were made to investigate the characteristics of the KUG. These are a radio continuum study of 38 selected objects (Maehara *et al.* 1985), an optical spectroscopic study of 57 selected objects (Maehara *et al.* 1987), optical and H I observations of four selected objects (Maehara *et al.* 1988), and optical and H I observations of 142 compact-morphology objects (Augarde *et al.* 1994; Comte *et al.* 1994). The results revealed that the KUGs are similar to the Markarian galaxies (Mazzarella, Balzano 1986) and most of the KUGs are actively star-forming galaxies. However, these previous studies did not examine the whole KUG sample; the samples used were much smaller in number compared with the total number of the KUG of 8162, or taking only a subsample with a certain morphology.

In this paper, using known optical color data, morphological data, and far-infrared data of a large number of the KUGs, we clarify the general characteristics of the KUGs quantitatively. We describe the sample and data in section 2. The optical colors and the morphological characteristics in connection with the Hubble system are given in section 3. In section 4, we discuss the nature of the KUGs by analyzing the optical luminosity functions, the far-infrared data, and some KUGs in Coma cluster. A summary is given in

section 5.

2. Data Description

The KUG survey was carried out in 170 Schmidt fields so far. Each field has a view of $5.7^\circ \times 5.7^\circ$, about 32 deg^2, and the total area of the survey is about 5100 deg^2, or 1.55 steradian. The total number of KUGs is 8162. A map of the surveyed regions was presented in figure 1 of TM93. TM93 noted that the KUG survey is not homogeneous in depth from the survey plate to plate; the limiting magnitude varies from $m_{pg} = 16.5$ to 18 mag depending on the plate quality. In order to avoid the effect of the inhomogeneity, we restrict a KUG sample used in this paper to those contained in the Zwicky catalog (Zwicky *et al.* 1961 – 1968 [CGCG]; hereafter CGCG galaxies), because the limiting magnitude of the CGCG galaxies is $m_{mg} = 15.7$, much less deep than that of the KUGs; hereafter we simply call them KUGs. We make a reference sample which are CGCG galaxies not selected as KUGs in the KUG-survey regions; we call them non-KUGs. Among all 170 KUG-survey fields, there are eight southern fields out of the CGCG-survey region of $\delta > -5^\circ$. The A0432 region (center position: $16^{\rm h}20^{\rm m}$, $+ 35^\circ$) is excluded in the following analyses because of the failure of the survey (Miyauchi-Isobe, Takase, Maehara 1997). Thus we take 161 fields out of 170. There are 2374 KUGs and 5797 non-KUGs in these regions.

We take the data for optical colors and Hubble-system morphological types, T index, from the RC3 (de Vaucouleurs *et al.* 1991). Therefore, our sample is restricted to those which are cataloged in the RC3. From the KUG catalog, we take the KUG morphology and the UV degree, which are given for all KUGs. We use the $IRAS$ data, therefore, we exclude objects located at the $IRAS$ non-survey regions and close binary galaxies to each of which the $IRAS$ measurements can not assign the far-infrared fluxes. The numbers of KUGs and non-KUGs in our sample become 1246 and 2804, respectively. Note that all of

the objects do not always have full listings in data.

3. Optical Characteristics of the KUGs

3.1. Color Difference between the KUGs and the non-KUGs

Since the picking up of the KUGs was made referring to colors of A0 stars on the same plate, the selection of the KUGs was little affected by the Galactic extinction; in analyzing the color data, we use mainly the color systems without the extinction correction. Figure 1 shows the color histograms for the KUG (solid lines) and the non-KUG (dashed lines) samples in $(U-B-V)_{\rm T}$ system. Each histogram is normalized to the total number of each sample. The color distributions differ between the KUGs and the non-KUGs. The number of objects, mean color, standard deviation of the distribution, and the colors at 20% and 80%-level of frequency distribution in each color system are summarized in table 1. We indicate an arrow in each histogram as the boundary between KUG and non-KUG colors, at which the fraction of KUGs with redder colors is equal to that of non-KUGs with bluer colors. We call the fraction of KUGs with the non-KUG colors, or the fraction of non-KUGs with the KUG colors, the overlapping fraction, which are 21% to 23% for all the colors. The boundary colors are 0.10 in $(U-B)_{\rm T}$ and 0.74 in $(B-V)_{\rm T}$. The color at the boundary and the overlapping fraction in each color are shown in the last two columns of table 1. These are the first quantitative expressions for the color criterion for the KUG.

Though the overlapping fractions are less than one fourth, the colors of the overlapped regions in the KUG sample extend up to the peak colors in the non-KUG sample. This may be due to the property of the survey procedure, i.e., eye-inspection of the three-image plates. For instance, the KUG survey might pick up objects with blue knots which are not always blue in total color.

Figure 2 shows $U-B$ versus $B-V$ color-color diagram for the KUGs and the non-KUGs. Figure 2a shows in $(U-B-V)_{\rm T}$ system. Circles indicate the KUGs of which both $(U-B)_{\rm T}$ and $(B-V)_{\rm T}$ colors are given in the RC3, 216 objects out of total 1246, and crosses indicate the non-KUGs, 427 objects out of total 2804. The boundary between KUG and non-KUG regions is shown as a dashed line, which has been defined in figure 1 to be the boundary color of $(U-V)_{\rm T}=0.83$. Figure 2b shows the color variation of the sample galaxies of both the KUGs and the non-KUGs along the morphology sequence in the Hubble system. The positions of dots indicate the mean colors and the error bars indicate the standard deviations of the color distributions. The color data and binning of the morphological types are summarized in table 2. From figures 2a and 2b, we find that the colors of the KUGs correspond to those of Sc or later-type galaxies.

Figures 2c is the same as figure 2b, but for the $(U-B-V)^0_{\rm T}$ system. The numbers of plotted galaxies, having both $(U-B)^0_{\rm T}$ and $(B-V)^0_{\rm T}$ colors in the RC3, are 208 and 403 for KUGs and non-KUGs, respectively. The boundary between KUG and non-KUG regions indicates the relation of $(U-V)^0_{\rm T}=0.64$, which is derived by the same procedure as made in $(U-V)_{\rm T}$ system. The colors of the main sequence stars are plotted in figure 2c following Allen (1973). Though the KUG colors were originally intended to be bluer than or equal to those of A0 stars, the color boundary has actually corresponded to G0 stars.

The KUG researchers introduced the UV degree, i.e., blueness, of the KUG images into three classes, H, M, and L from high to low. Figure 3 shows the color distribution of the sample in each UV degree in two color systems, $(U-B)_{\rm T}$ and $(B-V)_{\rm T}$. The number of sample, mean color, and standard deviation of the color distribution is summarized in table 3. The mean $(B-V)_{\rm T}$ colors for the H, M, and L samples are 0.48, 0.54, and 0.67, respectively, showing a correlation between the UV degree and the total colors. However, the correlation is not tight as shown in figure 3; this may be due to the property of the KUG

survey procedure. Though the colors of the KUGs with the UV degree of L overlaps those of the non-KUGs, the mean colors of L are still bluer than the boundary colors separating the KUGs from the non-KUGs; for instance, the mean $(B-V)_{\rm T}$ color for objects with L is 0.67, while the boundary color is 0.74.

3.2. KUG Fraction as a Funcion of the Hubble Sequence

The fraction of the KUG for each T index along the Hubble sequence is tabulated in table 4. The binning of the T index is shown in the first column. Another notation for the morphology is shown in the second column; -5: E, -2: S0, 1: Sa, 3: Sb, 5: Sc, 7: Sd, 9: Sm, 10: Im, 11: cI (no object in our sample), 90: I0, and 99: peculiar. Figure 4 illustrates the data in table 4. The abscissa indicates the T index of morphology given in the RC3; -6 to 11, one space, 90 and 99, and one space. The solid histogram indicates the KUGs in number and the dashed histogram indicates the total sample in number. The number scale is shown in the left-side ordinate. The solid broken line indicates the KUG fraction along the Hubble sequence. The scale for the fraction in % is shown in the right-side ordinate. In number, 54% of the KUGs with $-6 \leq T < 11$ have the Hubble types with $3 \leq T < 7$; a majority of the KUGs are spirals of Sb or Sc.

The fraction is monotonously increasing from early to late types. For E/S0 galaxies ($T < 0$) the fraction is less than 10%, on the other hand, for Sd – Im galaxies ($T = 7$ – 10) the fraction is about 50%. For $T \geq 5$ (later than or equal to Sc), the fraction exceeds 40% and this trend is consistent with the results by the color analysis given in section 3.1, i.e., the colors of the KUGs are bluer than or equal to those of Sc. However, we should note the following two points. Though the number is small, some E/S0 galaxies are recognized as KUGs. Though the fraction is high, about a half of Sd – Im galaxies are not recognized as KUGs.

Figure 5 shows the frequency of the UV degree along the Hubble sequence, and the data for figure 5 is also tabulated in table 4. The fraction of objects with higher UV degrees is monotonously increasing with the T index. It is found from figures 2, 4, and 5 that the KUGs are biased to the late-type galaxies in the Hubble sequence, and another contribution to the KUGs are galaxies with young star population regardless of the Hubble type.

Picking up of the KUG may be affected by the galaxy morphology as is mentioned in section 3.1; objects with blue knots may tend to be picked up, even if they are red in total color. The $(B-V)_{\rm T}$ color distribution for objects with the UV degree of M is shown in figure 6 and tabulated in table 5 along the Hubble sequence. A color variation is found in figure 6; the later the Hubble type is, the bluer the color is. The earliest category, $-6 \leq T < 2$, has a mean color of 0.66, while the latest category, $7 \leq T \leq 11$, has a mean color of 0.46, which is 0.2 mag bluer than the former one. This means that the early-type KUGs tend to show the peculiar features of having blue knots in red disks or bulges.

The color difference in $(B-V)_{\rm T}$ of 0.2 mag between the earliest and the latest KUGs is smaller than that of 0.5 mag in the non-KUGs as shown in the fifth column of table 5. Table 5 shows that the color difference between the KUG and the non-KUG becomes larger in earlier-type galaxies; the color difference is larger than 0.2 mag for galaxies with $T < 5$, and it reduces to less than 0.04 mag for galaxies with $T \geq 5$. This suggests that the late-type KUGs consist of mostly normal galaxies for their morphologies in terms of the stellar population, while the early-type KUGs consist of galaxies containing much young star populations for their morphologies.

3.3. Morphological Characteristics of the KUGs

The KUG catalog provides an original morphological classification (Takase, Noguchi, Maehara 1983) as follows; Ic is an irregular galaxy with clumpy H II regions, Ig is an irregular galaxy with a conspicuously giant H II region, Pi is a pair of interacting components, Pd is a pair of detached components, Sk is a spiral galaxy with knots of H II regions along arms, Sp is a spiral galaxy with peculiar bar and/or nucleus, C is a compact galaxy, and '?' is an unclassifiable one. TM93 summarized the frequency of the KUG morphological system and that of the UV degree in each KUG morphological type. In all following morphological analyses, we include objects with suspect classification; for instance, subsample with Ic is a combined sample of objects assigned originally as 'Ic' and 'Ic:'.

The correlation between the KUG morphology and the Hubble system, T index, is tabulated in table 6. It is found from table 6 that spiral KUGs with $0 \leq T < 9$ (S0a to Sdm) are mostly classified as Sk or Sp, i.e., they have knots of the H II regions in spiral arms or have peculiar bars or nuclei, showing that the selection of spiral KUGs were performed to be matched to these morphologies. This makes the KUG fraction suppressed to about a half even in late-type spirals by excluding the spirals with smoother features in blue light, though there is no difference in the stellar population between the late-type KUGs and the late-type non-KUGs as mentioned in section 3.2. In the case of later KUG with $9 \leq T < 11$ (Sm and Im), contribution of irregular or interacting features is larger. The earlier KUG with $T < 0$, the fraction of objects with C and Sp is larger, indicating the peculiar features, which is consistent with the indication that the early-type KUGs tend to have blue knots in red disks or bulges as mentioned in section 3.2.

It is found from table 6 that most of objects with C are unclassified in the Hubble system and about a half of galaxies in the C sample with known Hubble types are E/S0

galaxies. Comte *et al.* (1994) argued that the C sample consists of distant early-type galaxies. The radial velocity data of $V_{\rm GSR}$ in the RC3, a velocity system measured in the Galactic Standard of Rest, is given for 104 objects with C out of total 107. The mean radial velocity for the C sample is $V_{\rm GSR} = 5928$ km s^{-1}, similar to that for the total sample, $V_{\rm GSR} = 5224$ km s^{-1}; the C sample is not distant galaxies among the KUGs. Augarde *et al.* (1991) showed that most of the KUGs have the equivalent widths of the Hβ emission smaller than 15 Å, which are much smaller than that for I Zw 18 of 40 Å. Comte *et al.* (1994) showed that Hβ equivalent widths of the KUGs are systematically smaller than those of the blue galaxy sample given by the group at the University of Michigan, and they claimed that the KUGs are not strong star-forming galaxies. However, we should note that their sample is biased on KUGs with morphology of C. There are KUGs without the KUG morphology, though the sample number is small compared with to total number (see table 6). The distribution of their T index is flat from E to Im avoiding the mid-type spirals, Sb to Sc; this is the inverse trend of the distribution for the total sample. The mean radial velocity of the unclassifiable objects is $V_{\rm GSR} = 5274$ km s^{-1}, nearly the same as the mean value for the total sample. Therefore, their distances are not too distant to make the classification difficult.

4. Discussion

4.1. Luminosity Function of the KUGs

We investigate the difference of luminosity functions between the KUG and the non-KUG samples. We made the luminosity functions in a way as follows.

We consider B-band luminosity L_B derived from $B^0_{\rm T}$. The RC3 gives both values of $B^0_{\rm T}$ and $V_{\rm GSR}$ for 846 galaxies out of 4050 of the total KUG and non-KUG sample. Figure 7

shows the distribution of radial velocity of the sample in a bin of 1000 km s^{-1}. The solid curve indicates the canonical N-z relation expected for a uniform distribution of galaxies, drawn by using the Schechter-type luminosity function (Schechter 1976) with parameters given by Efstathiou, Ellis, Peterson (1988) and the limiting magnitude of 14.2 mag, and normalized by number. The overabundance at $V_{\rm GSR} < 2000$ km s^{-1} is partially due to the Virgo cluster.

Figure 8 shows the histogram of $B^0_{\rm T}$ magnitude of a combined sample of the KUGs and the non-KUGs in a bin of 0.2 mag. The data number used for figure 8 is 3391 out of 4050 of the total sample. The ordinate is shown in logarithmic scale. In a range from 11 to 14 mag, the number distribution is expressed in a single power-law, $\log N \propto$ dex $(0.5B^0_{\rm T})$, a little shallower than a canonical value of dex $(0.6B^0_{\rm T})$ which is expected for a complete uniform distribution. The shallower slope may correspond to the overabundance of near galaxies of $V_{\rm GSR} < 2000$ km s^{-1} as shown in figure 7. The power law is followed down to $B^0_{\rm T} = 14.2$ mag, therefore, we take $B^0_{\rm T} = 14.2$ as a limiting magnitude for completeness.

We use a relation between the B-band magnitude $B^0_{\rm T}$ and B-band luminosity L_B,

$$\log L_B\ [L_\odot] = -0.4\ B^0_{\rm T} + 2\ \log d\ [\rm Mpc] + 11.968,$$

which was used in Tomita, Tomita, Saitō (1996), where d is the distance to the galaxy in Mpc. We define the distance to the galaxy from $V_{\rm GSR}$,

$$d\ [\rm Mpc] = V_{\rm GSR}\ [\rm km\ s^{-1}]\ /\ 75.0.$$

If $V_{\rm GSR}$ is less than 75 km s^{-1}, we assign a distance of 1 Mpc. The distance where a galaxy with a luminosity of L_B is observed as a 14.2-mag object in $B^0_{\rm T}$, $d_{\rm max}$, is expressed as

$$\log d_{\rm max}\ [\rm Mpc] = 0.5\ \log L_B\ [L_\odot] - 3.144.$$

We restricted objects of which the distance is less than $d_{\rm max}$ defined above. For a given

luminosity, we define a volume, $(4\pi d_{\rm max}^3/3)(\Omega/4\pi)$, in which we can surely observe a galaxy with the luminosity; where Ω is the solid angle of the effective surveyed area for our sample galaxies and we take $\Omega = 1.4$ sr. Dividing the number of galaxies in each luminosity bin by the volume defined above, we made a luminosity function.

Figure 9 shows the luminosity functions for the KUG sample (solid line) and the non-KUG sample (dashed line). The abscissa indicates log L_B $[L_\odot]$ and the ordinate indicates the number of galaxies per Mpc^3 in a bin of 1 mag. The solid curve indicates the canonical luminosity function drawn by using the Schechter function (Schechter 1976) with parameters given by Efstathiou, Ellis, Peterson (1988). The luminosity functions of the KUGs and the non-KUGs also show a Schechter-like behavior and the luminosity function of a combined sample of the KUGs and the non-KUGs matches the canonical one well. For log $L_B < 10$, the slope and amplitude of the luminosity function are the same for both the KUG and non-KUG samples. The number densities of KUG and non-KUG are the same in this luminosity range. On the other hand, the luminosity function of the KUGs falls faster than that of the non-KUGs for log $L_B \geq 10$. In this luminosity range, the number density of the KUGs is several times lower than that of the non-KUGs; the KUGs are preferably less luminous galaxies with log $L_B < 10$.

Figure 10 shows the luminosity functions of the subsamples of the KUGs; four subsamples divided by the Hubble-type morphology, $-6 \leq T < 2$ (Sa or earlier), $2 \leq T < 5$ (Sb or Sbc), $5 \leq T < 7$ (Sc or Scd), and $7 \leq T \leq 11$ (Sd or later). The numbers of the samples are 78, 110, 131, and 94, respectively. The dashed histogram shows the luminosity function of the total KUG sample. Even for the KUGs, each morphological category shows a specific shape of the luminosity function as presented by Bingelli, Sandage, Tamman (1988). The luminosity function for the sample of Sa or earlier has a steep extension in log $L_B < 9$ and this is caused by the population of dwarf ellipticals. Figure 11 shows the

relative fraction of the subsamples drawn by using the data in figure 10. For log $L_B \geq 9.4$, a combined sample of Sb to Scd dominates. The KUGs with luminosities at around the knee of the KUG luminosity function are mostly mid-type spirals. For log $L_B \leq 9.3$ the dwarf population, the sample of Sd or later and the sample of dwarf ellipticals, dominate.

The apparent KUG fraction would decrease with distance since the KUG fraction decreases with increasing luminosity as shown in figure 9. Figure 12 shows the KUG fraction as a function of $V_{\rm GSR}$ in a bin of 1000 km s^{-1}. For galaxies with $V_{\rm GSR} < 4000$ km s^{-1}, the KUG fractions are higher than 40%, which is consistent with the fact that the number densities of the KUGs and the non-KUGs are similar to each other for fainter galaxies. The KUG fraction decreases steeply in a range of $V_{\rm GSR} = 4000$ km s^{-1} to 6000 km s^{-1}. For galaxies with $V_{\rm GSR} = 6000$ to 13000 km s^{-1}, the KUG fractions are about one fourth, which is consistent with that the number density of the KUGs are several times smaller than that of the non-KUGs for galaxies brighter than $L_B > 10^{10} L_\odot$. At $V_{\rm GSR} = 6000$ km s^{-1}, the distance is assumed to be 80 Mpc, a galaxy with log L_B $[L_\odot] = 10$ would be seen as an object with $B_{\rm T}^0 = 14.4$, which is nearly the completeness limit of our sample (see figure 8). The variation of the KUG fraction with distance is consistent with the difference of luminosity functions of the KUGs and the non-KUGs.

4.2. Far-Infrared Characteristics of the KUGs

The far-infrared (FIR) emission measured by *IRAS* has been used as an indicator for the star formation (e.g., de Jong *et al.* 1984; Soifer *et al.* 1987; Bothun, Lonsdale, Rice 1989), though is has been pointed out that radiation from old stellar populations should contribute to the total FIR emission in the galaxy (e.g., Sauvage, Thuan 1992; Walterbos, Greenawalt 1996). Tomita, Tomita, Saitō (1996) showed that the FIR-to-B band flux ratio, f_{FIR}/f_B, is a useful measure of the present star formation activity in galaxies. They

studied the variation of the activity in spiral galaxies analyzing as many as 1681 spirals and found that the range of log f_{FIR}/f_B is from -1.5 to 0.5. Spirals with log $f_{FIR}/f_B > 0$ thus represent the very active subsample. Following the method used in Tomita, Tomita, Saitō (1996), we calculated f_{FIR}/f_B for our sample. The data of f_{FIR} was taken from $IRAS$ catalogs, PSC, FSC, SSSC, and CGQIRAS, and Rice *et al.* (1988) and Soifer *et al.* (1987). Since we adopted $B^0_{\rm T}$ system for the B-band magnitude, only objects with measured $B^0_{\rm T}$ in the RC3 are considered here; the numbers of them are 592 and 1397 for the KUG and the non-KUG samples, respectively. Among them 378 of the KUG sample and 514 of the non-KUG sample have measured values of f_{FIR}/f_B and others have only upper-limit values of f_{FIR}/f_B because of non-detection of the $IRAS$ measurements.

Figure 13 shows the distribution of log f_{FIR}/f_B showing in each Hubble morphological type. The left-side panels indicate the KUG samples and the right-side panels indicate the non-KUG samples. The solid histograms show the samples with measured f_{FIR}/f_B and the dashed ones show those with only upper-limit values of f_{FIR}/f_B. Note that each histogram is a simple frequency of our sample and not one for a volume-limit sample as presented in Tomita, Tomita, Saitō (1996). With a bias that FIR-bright objects can be seen from more distant places, the simple histogram may shift to a higher value in f_{FIR}/f_B compared with one for a volume-limit sample.

It is found from figure 13 that the KUG samples have several times larger values of f_{FIR}/f_B than the non-KUG samples for E/S0 and Sa. On the other hand, the distributions of the KUG and the non-KUG samples in f_{FIR}/f_B are similar to each other for Sb or later-type categories. The fraction of galaxies showing intense activity, here we take those with log $f_{FIR}/f_B \geq 0$, is larger in the KUG sample than in the non-KUG sample for all the morphological types and especially it is remarkable for E/S0 and Sa samples.

Figure 13 shows a trend that the median value of f_{FIR}/f_B is decreasing from early to

late types of the KUG sample. The flux ratio of f_{FIR}/f_B is the luminosity ratio of L_{FIR}/L_B. Taking the far-infrared luminosity, L_{FIR}, is a measure of the present star formation rate (SFR) (Devereux, Young 1991; Sauvage, Thuan 1992), SFR is expressed as

$$\text{SFR } [M_\odot \text{ yr}^{-1}] = 1.4 \times 10^{-10} \; L_{FIR} \; [L_\odot].$$

Assuming that the age of the galaxy is 10^{10} yr and that the luminous-to-dark mass ratio is unity as suggested by Rubin (1987), the past average SFR, <SFR>, is expressed as M_T / 2×10^{10}. Then,

$$\text{SFR / <SFR>} = 2.8 \; L_{FIR}/M_T.$$

The B-band luminosity, L_B, is affected by the star formation history (e.g., Gallagher, Hunter, Tutukov 1984), though it is nearly a measure of the galaxy mass (e.g., Hodge 1993). We make a color-dependent M_T/L_B using M_T/L_B and $(B-V)^0_{\rm T}$ data for 245 galaxies in Nearby Galaxies Catalog (Tully 1988 [NBGC]) with morphologies of $T = 1$ – 8. The extinction correction is made for the B-band luminosity cataloged in the NBGC. Excluding nine objects by the 3-σ rejection, we got a relation,

$$\log \, (M_T/L_B) \; [M_\odot \; / \; L_\odot] = 0.847 \; (B-V)^0_{\rm T} + 0.188 \pm 0.191.$$

These two equations yield a relation,

$$\log \, (\text{SFR / <SFR>}) = \log \, (f_{FIR}/f_B) - 0.847 \; (B-V)^0_{\rm T} + 0.635.$$

The mean values of $(B-V)^0_{\rm T}$ for E/S0, Sa, Sb, and Sc in the KUG sample are 0.73, 0.58, 0.56, and 0.49, respectively. Then we found that the median value of log L_{FIR}/M_T is around -0.9 regardless of the morphology, and that the median value of the present-to-past SFR for the KUGs is derived to be about 0.4. Kennicutt, Tamblyn, Congdon (1994) studied the present-to-past SFR which they called b-parameter. Though we need attention in comparison between our rough estimation and their calculations because their analysis

was careful by taking into account the gas recycling process, our preset-to-past SFR of 0.4 is larger than their values for Sb or earlier-type galaxies (see their figure 6).

4.3. Post-Starburst Galaxies in the KUGs

The KUGs appear even in early-type galaxies and these are blue for their Hubble-type morphology as described in section 3. We show that post-starburst galaxies contribute to the early-type KUGs.

Takase (1980) showed the spatial distribution of the KUGs in Coma cluster field (see figure 2 of his paper). The KUGs exist even in the central region of Coma cluster, though the number is small. Caldwell *et al.* (1993) presented a number of spectra of Coma cluster members with early-type morphologies to investigate 'abnormal' spectra, which have strong Balmer absorption lines (see figure 17 of their paper). These spectra resemble the E+A spectra for galaxies at distant clusters which are interpreted as post-starburst galaxies related to the Butcher-Oemler effect (Dressler, Gunn 1983; Butcher, Oemler 1984). Among about 500 galaxies of Takase (1980), which contains both KUGs and non-KUGs down to $m_{pg} = 18$ in Coma, we noticed twelve galaxies having the abnormal spectra or strong Hδ absorption by inspecting the data given by Caldwell *et al.* (1993). Table 7 tabulated the data of the twelve galaxies; the galaxy ID-number given in Goldwin, Metcalfe, Peach (1983), b magnitude, $b - r$ color, and equivalent width of the Hδ in the unit of Å given in Caldwell *et al.* (1993), and cross-identification with KUG and Markarian catalogs. Only one object, KUG 1256+278B, is included in our total sample of 4050 and its T index is -3.0. T indices of other four KUGs are unknown. However, all of them are recognized as early-type galaxies by Caldwell *et al.* (1993).

Table 7 shows a clear relation among KUG, Markarian, and post-starburst galaxies.

The KUG survey picked up all galaxies with abnormal spectra with EW(Hδ absorption) $\geq$ 3.5 Å, and no galaxies with EW(Hδ) $<$ 3.5 Å were recognized as KUGs. Markarian galaxies correspond to KUGs with the UV degree of M and have more strict criterion than KUG in a sense that the objects with EW(Hδ) $\geq$ 4.5 Å match the Markarian galaxies. The three galaxies in table 7 following top two Markarian galaxies are enough bright to be picked up as the Markarian galaxies. This means that the KUG catalog is not a simple extension to fainter magnitude of the Markarian catalog and that the KUG survey picked up the post-starburst galaxies more effectively. The spectral feature of the post-starburst galaxies, blue SED (spectral energy distribution) without strong emission lines, passes the KUG criteria more effectively.

In the Local Universe, only several post-starburst galaxies are reported so far (e.g., Walker, Lebofsky, Rieke 1988; Zabludoff *et al.* 1996). The post-starburst galaxies may be common among the blue galaxies in the Local Universe as is at intermediate redshifts (e.g., Dressler, Gunn 1988).

5. Summary

We analyze 1240 KUGs comparing with 2804 non-KUGs to investigate the characteristics of the KUGs.

1. We introduced the quantitative expressions for the KUG criteria for the first time. The boundary colors separating the KUGs from the non-KUGs are 0.10 and 0.74 in $(U-B)_{\rm T}$ and $(B-V)_{\rm T}$, respectively. The overlapping fractions in colors between the KUGs and the non-KUGs are 21 to 23%. The mean colors in $(B-V)_{\rm T}$ for objects with the UV degree of H, M, and L are 0.48, 0.54, and 0.67, respectively.

2. The colors of the KUGs correspond to those of Sc or later-type galaxies in the

Hubble sequence. The boundary color corresponds to that of a G0 star of the main sequence.

By our quantitative analysis, the KUGs are clearly shown to be a sample of blue galaxy population. The results and discussion given for the KUGs, summarized below, are for the blue galaxy population in general.

3. More than a half of the KUGs with known Hubble-type morphology are Sb to Scd ($3 \leq T < 7$). The dwarf irregulars do not dominate in number because of their low luminosities.

4. The KUGs prefer late-type spirals in the Hubble system and the KUG fraction changes linearly along the Hubble sequence; it is less than 10% for E/S0 and more than a half for Sd/Sm.

5. In terms of the stellar population the late-type KUGs are normal galaxies and the early-type KUGs are peculiar galaxies. The color difference between the KUGs and the non-KUGs is negligible for the KUGs with $T \geq 5$, while it is significant for the KUGs with $T < 5$; the early-type KUGs have much young star populations for their morphologies. We analyzed the data of f_{FIR}/f_B, a measure of the present star formation activity in galaxies. It was found that for Sb or earlier-type categories, the KUG sample shows several times more intense activity than the non-KUG sample. In the late-types, the KUGs have similar star formation history and present star formation activity to the non-KUGs. We calculated L_{FIR}/M_T and found that the typical value of the present-to-past star formation rate for the KUGs is 0.4 and nearly constant in any Hubble morphology.

6. The early-type KUG sample also contains the post-starburst galaxies with EW(Hδ absorption) ≥ 3.5 Å; such objects are more effectively picked up in the KUG survey than in the Markarian survey. It has been argued that the post-starburst galaxies among the blue

galaxies are found preferably at a cosmological distance. The KUGs, the local counterpart of the blue galaxies, surely contains the post-starburst galaxies, though the quantitative fraction is not clear so far.

7. In the late-type morphology, the KUGs show more knotty morphology in blue light than the non-KUGs, though the stellar populations are similar to each other. The early-type KUGs have blue knots in their red disks or bulges and this peculiar morphology is related to the intense star formation activity for their Hubble type.

8. The KUGs are biased to less luminous galaxies. We analyzed the luminosity functions of the KUG and the non-KUG samples. For $\log L_B < 10$, the number density of the KUG and the non-KUG are similar to each other. For $\log L_B \geq 10$, the number density of the non-KUG is several times larger than that of the KUG. This is also consistent with the selection effect in the KUG fraction due to distance. Being less luminous tends to lead to the intense star formation in earlier Hubble types. At around the knee of the luminosity function of the KUGs, most of the KUGs are spiral galaxies. Dwarf population dominates in fainter class of $\log L_B \leq 9.3$.

9. The fraction of the blue population in a survey depends on the depth of the survey. If the survey is enough deep to pick up most of the dwarf population, the fraction would be high; this is another bias to be considered for the fraction of the blue population in a cosmologically deep survey as well as the evolutionary effect.

One of the authors (TTT) acknowledges the Research Fellowships of the Japan Society for the Promotion of Science for Young Scientists. This research has also made use of the NASA/IPAC Extragalactic Database (NED) which is operated by the Jet Propulsion Laboratory, Caltech, under contact with the National Aeronautics and Space Administration. Finnaly, We are grateful to the anonymous referee for improving the paper.

REFERENCES

Allen, C. W. 1973, *Astrophysical Quantities Third Edition* (The Athlone Press, University of London, London)

Augarde, R., Comte, G., Chalabaev, A., Kunth, D., Maehara, H. 1991, in Primeval Galaxies and Related Problems, Proceedings of Japan-France Seminar, Annales de Physique, 16, 105

Augarde, R., Chalabaev, A., Comte, G., Kunth, D., Maehara, H. 1994, A&AS, 104, 259

Binggeli, B., Sandage, A., Tamman, G. A. 1988, ARA&A, 26, 509

Bothun, G. D., Lonsdale, C. J., Rice, W. 1989, ApJ, 341, 129

Butcher, H., Oemler A., Jr. 1984, ApJ, 285, 426

Caldwell, N., Rose, J. A., Sharples, R. M., Ellis, R. S., Bower, R. G. 1993, AJ, 106, 473

Cataloged Galaxies and Quasars Observed in the IRAS Survey 1985, prepared by Lonsdale, C. J., Helou, G., Good, J., Rice, W. (JPL, Pasadena) [CGQIRAS]

Comte, G., Augarde, R., Chalabaev, A., Kunth, D., Maehara, H. 1994, A&A, 285, 1

de Jong, T., Clegg, P. E., Soifer, B. T., Rowan-Robinson, M., Habing, H. J., Houck, J. R., Aumann, H. H., Raimond, E. 1984, ApJ, 278, L67

de Vaucouleurs, G., de Vaucouleurs, A., Corwin, H. G., Jr., Buta, R. J., Paturel, G., Forqué, P. 1991, Third Reference Catalogue of Bright Galaxies (Springer-Verlag, New York) [RC3]

Devereux, N. A., Young, J. S. 1991, ApJ, 371, 515

Dressler, A., Gunn, J. E. 1983, ApJ, 270, 7

Dressler, A., Gunn, J. E. 1988, in Large Scale Structures of the Universe, IAU Symp. No. 130, ed Audouze, J. et al. (Kluwer, Dordrecht) p311

Efstathiou, G., Ellis, R. S., Peterson, B. A. 1988, MNRAS, 232, 431

Gallagher, J. S., III, Hunter, D. A., Tutukov, A. V. 1984, ApJ, 136, 748

Goldwin, J. G., Metcalfe, N., Peach, J. V. 1983, MNRAS, 202, 113

Hodge P. 1993, in Star Formation, Galaxies and the Interstellar Medium, ed Franco, J., Ferrini, F., Tenorio-Tagle, G. (Cambridge University Press, Cambridge) p294

IRAS Faint Source Catalog $|b| > 10$ *Degrees Version 2.0* 1989, prepared by Moshir, M. (GPO, Washington, DC) [FSC]

IRAS Point Source Catalog 1985, Joint *IRAS* Science Working Group (GPO, Washington, DC) [PSC]

IRAS Small Scale Structures Catalog 1986, prepared by Helou, G., Walker, D. W. (GPO, Washington, DC) [SSSC]

Kennicutt, R. C., Jr., Tamblyn, P., Congdon, C. W. 1991, ApJ, 435, 22

Maehara, H., Hamabe, M., Bottinelli, L., Gouguenheim, L., Heidmann, J. 1988, PASJ, 40, 47

Maehara, H., Inoue, M., Takase, B., Noguchi, T. 1985, PASJ, 37, 451

Maehara, H., Noguchi, T., Takase, B., Handa, T. 1987, PASJ, 39, 393

Mazzarella, J. M., Balzano, V. A. 1986, ApJS, 62, 751

Miyauchi-Isobe, N., Takase, B., Maehara, H. 1997, Publ. Natl. Astron. Obs. Japan, 4, 153

Rice, W., Lonsdale, C. J., Soifer, B. T., Neugebauer, G., Kopan, E. L., Lloyd, L. A., de Jong, T., Habing, H. J. 1988, ApJS, 68, 91

Rubin, V. C. 1987, in Dark Matter in the Universe, ed Kormendy, J., Knapp, G. R. (Dordrecht, Reidel) p51

Sauvage, M., Thuan, T. X. 1992, ApJ, 396, L69

Schechter, P. 1976, ApJ, 203, 297

Soifer, B. T., Sanders, D. B., Madore, B. F., Neugebauer, G., Danielson, G. E., Elias, J. H., Lonsdale, C. J., Rice, W. L. 1987, ApJ, 320, 238

Takase, B. 1980, PASJ, 32, 605

Takase, B., Noguchi, T., Maehara, H. 1983, Ann. Tokyo Astron. Obs. 2nd Ser., 19, 440

Takase, B., Miyauchi-Isobe, N. 1993, Publ. Natl. Astron. Obs. Japan, 3, 169 [TM93]

Tomita, A., Tomita, Y., Saitō, M. 1996, PASJ, 48, 285

Tully, R. B. 1988, Nearby Galaxies Catalog (Cambridge University Press, Cambridge) [NBGC]

Walker, C. E., Lebofsky, M. J., Rieke, G. H. 1988, ApJ, 325, 687

Walterbos, R. A. M., Greenawalt, B. 1996, ApJ, 460, 696

Zabludoff, A. I., Zaritsky, D., Lin, H., Tucker, D., Hashimoto, Y., Shectman, S. A., Oemler, A., Jr., Kirshner, R. P. 1996, ApJ, 466, 104

Zwicky, F., Herzog, E., Kowal, C. T., Wild, P., Karpowicz, M. 1961 – 1968, Catalogue of Galaxies and of Clusters of Galaxies (California Institute of Technology, Pasadena) [CGCG]

This manuscript was prepared with the AAS LaTeX macros v4.0.

Fig. 1.— Histograms of colors for the KUG and the non-KUG samples in $(U-B-V)_{\rm T}$ system. Solid one indicates the KUG sample and the dashed one indicates the non-KUG sample. Each histogram is normalized to the total number of the each sample. The abscissa is for the color and the color system used is shown in the upper left corner in the histogram. The ordinate is for the relative frequency in the unit of %. An arrow indicates the boundary color separating the KUG from the non-KUG samples. The characteristics of the histograms are also tabulated in table 1.

Fig. 2.— (a) $(U-B-V)_{\rm T}$ color-color diagram for the KUG and the non-KUG samples. Circles indicate the KUG sample and crosses indicate the non-KUG sample. The abscissa indicates $(B-V)_{\rm T}$ and the ordinate indicates $(U-B)_{\rm T}$ colors. Dashed line indicates the color boundary separating the KUG from the non-KUG samples, $(U-V)_{\rm T}=0.83$, given in table 1. (b) Color variation along the Hubble morphological sequence shown in $(U-B-V)_{\rm T}$ plane. The color data for each Hubble type was derived from a combined sample of the KUGs and non-KUGs. The data is also tabulated in table 2. The dashed line, the same as in figure 2a, shows the boundary color. The colors of the KUGs correspond to those of Sc or later-type galaxies. (c) The same as figure 2b, but in $(U-B-V)^0_{\rm T}$ plane. Dashed line indicates the boundary color of $(U-V)^0_{\rm T}=0.64$. Colors of the main sequence stars are plotted. The color boundary corresponds to that of G0 stars, though originally the color of the KUG criterion was intended to be A0 stars.

Fig. 3.— Color variation along the UV degree, H, M, and L. (a) Histogram shown in $(U-B)_{\rm T}$ and (b) in $(B-V)_{\rm T}$. Each histogram is normalized to the total number of each sample. The ordinate indicates the relative frequency in %. There is a correlation between the UV degree and the total colors, though the separation of color distribution is not clear. The mean color and the standard deviation of the distribution in each color system is tabulated in table 3. Note that the color with the UV degree of L is bluer than the boundary color separating the

KUG from the non-KUG samples.

Fig. 4.— The fraction of the KUG in a bin of the T index along the Hubble sequence drawn using the data in table 4. Solid histogram shows the number of the KUG and dashed one shows the number of the total samples. The scale of the number is shown in left-side ordinate. The abscissa indicates the Hubble morphological type, T index. A solid broken line shows the KUG fraction in a bin of the T index. The scale of the fraction in % is shown in right-side ordinate. The fraction is monotonously increasing along the Hubble type.

Fig. 5.— Variation of the relative frequency of the UV degree in each T index along the Hubble sequence. The fraction of the higher UV degrees is monotonously increasing with T index. The data is also tabulated in the last three columns of table 4.

Fig. 6.— $(B-V)_{\rm T}$ colors of objects with the UV degree of M for different Hubble morphological types. The ordinate indicates the relative frequency in each histogram. The most lower panel shows the histogram for the total sample with the UV degree M. The mean color and the standard deviation of the distribution of each histogram is tabulated in table 5.

Fig. 7.— Radial velocity $V_{\rm GSR}$ distribution of a combined sample of the KUGs and the non-KUGs. The velocity data was taken from the RC3. The number of data used is 846. The solid curve indicates the canonical N-z relation which is expected for a uniform distribution of galaxies.

Fig. 8.— $B^0_{\rm T}$ distribution of a combined sample of the KUGs and the non-KUGs. The data was taken from RC3. The number of data used is 3391. A single power-law of $\log N \propto (0.5B^0_{\rm T})$ follows down to $B^0_{\rm T} = 14.2$.

Fig. 9.— Log L_B luminosity functions for the KUG and the non-KUG samples. The solid

histogram is for the KUGs and the dashed one is for the non-KUGs. The solid curve indicates the Schechter-type canonical luminosity function.

Fig. 10.— The luminosity functions of the KUGs for four morphological subsamples; (a) samples with $-6 \leq T < 2$ (Sa or earlier) and $2 \leq T < 5$ (Sb or Sbc), and (b) $5 \leq T < 7$ (Sc or Scd) and $7 \leq T \leq 11$ (Sd or later). The dashed histogram shows the luminosity funciton of the total KUG sample as shown in figure 9.

Fig. 11.— The variation of the relative fraction of the KUGs in the four morphological categories along L_B; sample with $-6 \leq T < 2$ (denoted as E – Sa in the panel), $2 \leq T < 5$ (Sb), $5 \leq T < 7$ (Sc), and $7 \leq T \leq 11$ (Sd – Im).

Fig. 12.— The variation of the KUG fraction as a function of $V_{\rm GSR}$ in a bin of 1000 km s^{-1}. 0 – 1000 km s^{-1} bin contains galaxies with $V_{\rm GSR} < 1000$ [km s^{-1}], 1000 – 2000 km s^{-1} bin contains galaxies with $1000 \leq V_{\rm GSR} < 2000$ [km s^{-1}] and so on.

Fig. 13.— Distribution of far-infrared-to-B band flux ratio for each Hubble morphological type; E/S0: $T < 0$, Sa: $0 \leq T < 2$, Sb: $2 \leq T < 4$, Sc: $4 \leq T < 6$, Sd: $6 \leq T < 8$, and Sm/Im: $8 \leq T \leq 11$. The left-side panel indicates the KUG sample and the right-side panel indicates the non-KUG sample. The abscissa indicates the flux ratio in logarithmic scale and the ordinate indicates the relative frequency within each panel in %. The solid histogram shows the sample with measured values of f_{FIR}/f_B, and the dashed one shows the sample with only upper-limit values of f_{FIR}/f_B. Note that these histograms are simple frequency of our sample.

Table 1: Color differences between the KUG and the non-KUG samples.

Color	K U G					n o n - K U G					Boundary	
system	(1)	(2)	(3)	(4)	(5)	(1)	(2)	(3)	(4)	(5)	(A)	(B)
$(U-B)_{\rm T}$	216	−0.05	0.22	−0.22	0.10	427	0.30	0.24	0.09	0.51	0.10	21
$(B-V)_{\rm T}$	264	0.62	0.16	0.46	0.75	526	0.86	0.18	0.71	1.00	0.74	23
$(U-V)_{\rm T}$	216	0.56	0.36	0.26	0.83	427	1.16	0.41	0.81	1.51	0.83	21

Columns:
(1) Number of objects used
(2) Mean value of the color
(3) Standard deviation of the distribution
(4) Color at the 20-% level
(5) Color at the 80-% level
(A) The boundary color separating the KUG from the non-KUG samples
(B) The overlapping fraction in % between the KUG and the non-KUG samples

Table 2: Color variation along the Hubble morphological sequence.

Color		E	S0	Sa	Sb	Sc	Sd	Im
$(U-B)_{\rm T}$	number	67	127	60	97	94	40	62
	mean	0.45	0.44	0.24	0.21	0.01	−0.03	−0.18
	σ	0.15	0.15	0.25	0.19	0.16	0.13	0.16
$(B-V)_{\rm T}$	number	91	149	76	122	130	52	67
	mean	0.99	0.95	0.83	0.80	0.66	0.58	0.49
	σ	0.12	0.09	0.16	0.13	0.13	0.12	0.14
$(U-B)^0_{\rm T}$	number	66	121	60	96	95	40	62
	mean	0.46	0.44	0.18	0.09	−0.08	−0.09	−0.20
	σ	0.16	0.17	0.24	0.17	0.15	0.13	0.16
$(B-V)^0_{\rm T}$	number	87	140	74	117	128	52	67
	mean	0.91	0.89	0.71	0.65	0.54	0.51	0.46
	σ	0.10	0.08	0.15	0.13	0.13	0.11	0.13

Notes:
Ranges of T index: E: $-6 \geq T > -3$, S0: $-3 \geq T > 0$, Sa: $0 \geq T > 2$, Sb: $2 \geq T > 4$, Sc: $4 \geq T > 6$, Sd: $6 \geq T > 8$, and Im: $8 \geq T \geq 11$.

Table 3: Color variation along the UV degree.

Color	H			M			L		
system	(1)	(2)	(3)	(1)	(2)	(3)	(1)	(2)	(3)
$(U-B)_{\rm T}$	21	-0.28	0.24	64	-0.11	0.22	131	0.02	0.18
$(B-V)_{\rm T}$	26	0.48	0.13	75	0.54	0.14	163	0.67	0.15
$(U-V)_{\rm T}$	21	0.20	0.35	65	0.43	0.32	131	0.69	0.30

Columns:
(1) Number of objects used
(2) Mean value of the color
(3) Standard deviation of the distribution

Table 4: The fraction of the KUG along the Hubble sequence.

Range of T index		Total number	Number of KUG	Fraction of KUG	UV degree (number) H	M	L
$-6 \le T < -5$	cE	2	0	0.0	0	0	0
$-5 \le T < -4$	E	201	9	4.5	0	4	5
$-4 \le T < -3$	cD	27	1	3.7	0	1	0
$-3 \le T < -2$	$S0^-$	100	1	1.0	0	0	1
$-2 \le T < -1$	$S0^\circ$	291	23	7.9	4	10	10
$-1 \le T < 0$	$S0^+$	53	6	11.3	0	0	5
$0 \le T < 1$	S0a	145	17	11.7	0	3	14
$1 \le T < 2$	Sa	212	50	23.6	0	10	40
$2 \le T < 3$	Sab	193	36	18.7	1	8	27
$3 \le T < 4$	Sb	388	96	24.7	5	20	71
$4 \le T < 5$	Sbc	247	94	38.1	2	21	71
$5 \le T < 6$	Sc	145	64	44.1	7	13	44
$6 \le T < 7$	Scd	310	131	42.3	8	32	91
$7 \le T < 8$	Sd	111	49	44.1	4	19	26
$8 \le T < 9$	Sdm	102	54	52.9	3	32	19
$9 \le T < 10$	Sm	37	21	56.8	7	7	7
$10 \le T < 11$	Im	102	44	43.1	10	17	17
$T = 11$	cI	0	0	–	0	0	0
$T = 90$[a]	I0	6	2	33.3	0	0	2
$T = 99$[a]	Pec	17	13	76.5	2	5	60
(not given)[b]	?	1361	535	39.3	45	185	305
Total		4050	1246	30.8	98	387	761

[a] Fractions for these morphologies are not plotted in the broken line in figure 4.

[b] Data for objects without T index is not shown in figure 4.

Table 5: $(B-V)_{\rm T}$ color variation along the Hubble-type morphology for objects with the UV degree of M.

(1)	(2)	(3)	(4)	(5)
$-6 \leq T < 2$	13	0.66	0.16	0.97
$2 \leq T < 5$	13	0.61	0.14	0.81
$5 \leq T < 7$	14	0.52	0.08	0.68
$7 \leq T \leq 11$	15	0.46	0.10	0.48
Total[a]	75	0.54	0.14	

Columns:
(1) Range of T index
(2) Number of objects used
(3) Mean value of the color
(4) Standard deviation of the distribution
(5) Mean value of the color for the non-KUG sample

[a] All sample including objects without T index.

Table 6: The KUG morphology vs T index correlation.

Range of T index		KUG morphological type [a]								Total
		Ic	Ig	Pi	Pd	Sk	Sp	C	?	
$-6 \le T < -5$	cE	0	0	0	0	0	0	0	0	0
$-5 \le T < -4$	E	0	0	1	0	0	2	3	3	9
$-4 \le T < -3$	cD	0	0	0	0	0	1	0	0	1
$-3 \le T < -2$	$S0^-$	0	0	0	0	0	0	1	0	1
$-2 \le T < -1$	$S0^\circ$	1	0	3	0	7	4	5	3	23
$-1 \le T < 0$	$S0^+$	0	0	0	0	2	1	1	2	6
$0 \le T < 1$	S0a	0	0	1	1	7	6	2	0	17
$1 \le T < 2$	Sa	1	0	2	0	19	23	3	2	50
$2 \le T < 3$	Sab	1	0	2	1	18	13	1	0	36
$3 \le T < 4$	Sb	2	1	3	1	61	27	0	1	96
$4 \le T < 5$	Sbc	2	0	3	0	54	35	0	0	94
$5 \le T < 6$	Sc	5	1	2	1	41	14	0	0	64
$6 \le T < 7$	Scd	2	1	1	1	57	64	2	3	131
$7 \le T < 8$	Sd	2	0	2	0	17	26	1	1	49
$8 \le T < 9$	Sdm	2	1	3	0	18	26	1	3	54
$9 \le T < 10$	Sm	3	0	5	0	4	8	0	1	21
$10 \le T < 11$	Im	14	3	5	1	5	11	0	5	44
$T = 11$	cI	0	0	0	0	0	0	0	0	0
$T = 90$	I0	0	0	0	0	0	0	2	0	2
$T = 99$	Pec	3	2	0	0	1	3	2	2	13
(not given)	?	23	6	19	4	173	197	83	30	535
Total		61	15	52	10	484	461	107	56	1246

[a] Objects with suspected morphological classification are included.

Table 7: Characteristics of galaxies with abnormal spectra in Coma cluster.

GMP[a]	b	$b-r$	EW(Hδ)	KUG			Mrk
number			[Å][b]	name	mor	UV	
4918	16.03	1.47	4.54	1254+276	Pi	M	55
2897	16.98	1.53	4.51	1257+281	?	M	60
3896	15.13	1.75	4.04	1256+281	Sk	L	
4156	14.38	1.66	3.84	1256+278B	C	L	
4255	16.57	1.77	3.78	1256+278A	?	L	
2551	16.85	2.99	3.25				
4974	16.49	1.62	2.50				
5096	16.89	1.78	2.50				
2989	17.05	1.88	2.30				
4294	17.64	1.72	2.29				
4522	15.83	1.84	1.80				
3254	16.57	1.84	1.10				

[a] Galaxy ID-number given in Goldwin, Metcalfe, Peach (1983).

[b] The Hδ line is absorption in this case.

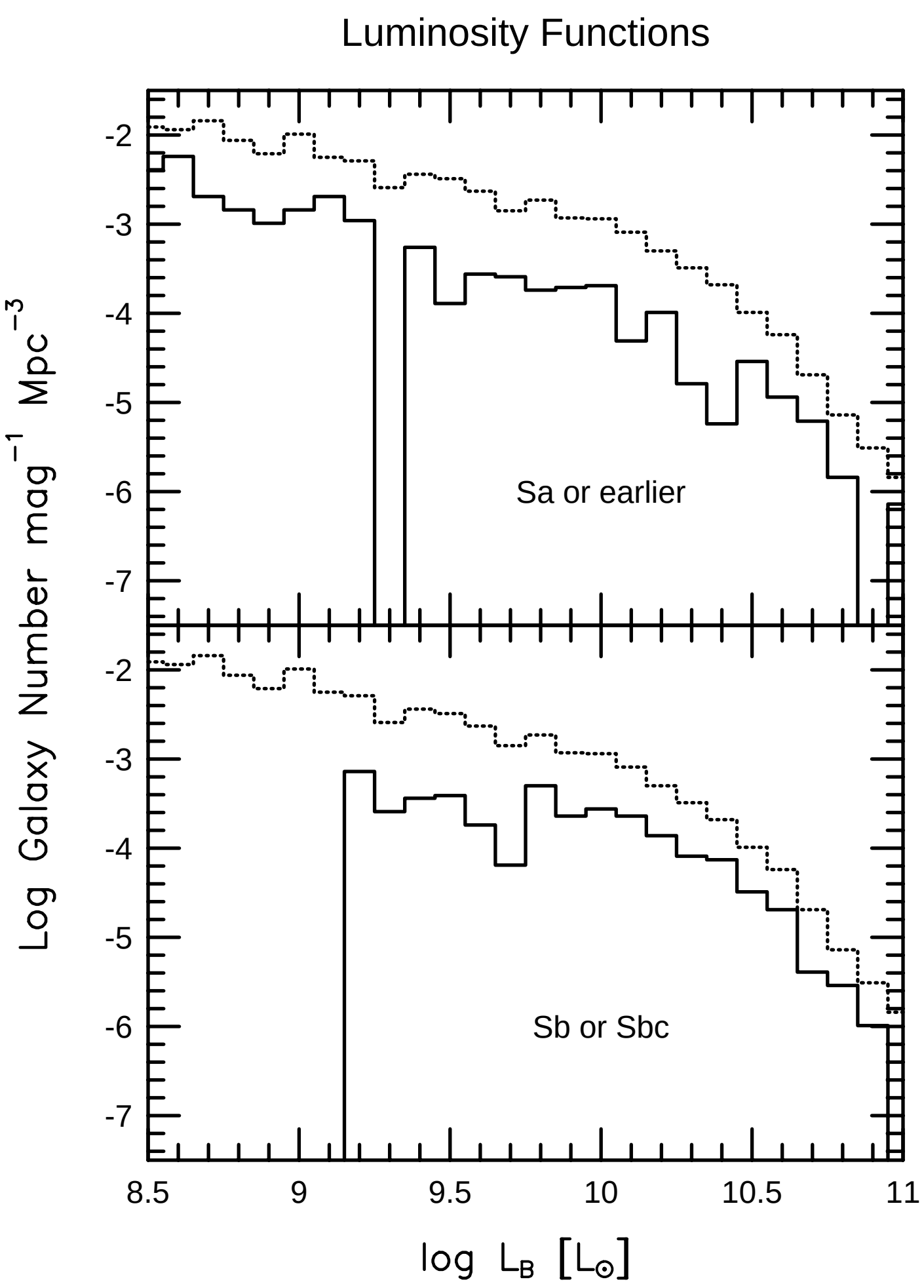
Luminosity Functions
Log Galaxy Number mag^{-1} Mpc^{-3}
-2
-3
-4
-5
-6
-7
Sa or earlier
Sb or Sbc
8.5
9
9.5
10
10.5
11
log L_B [$L_\odot$]

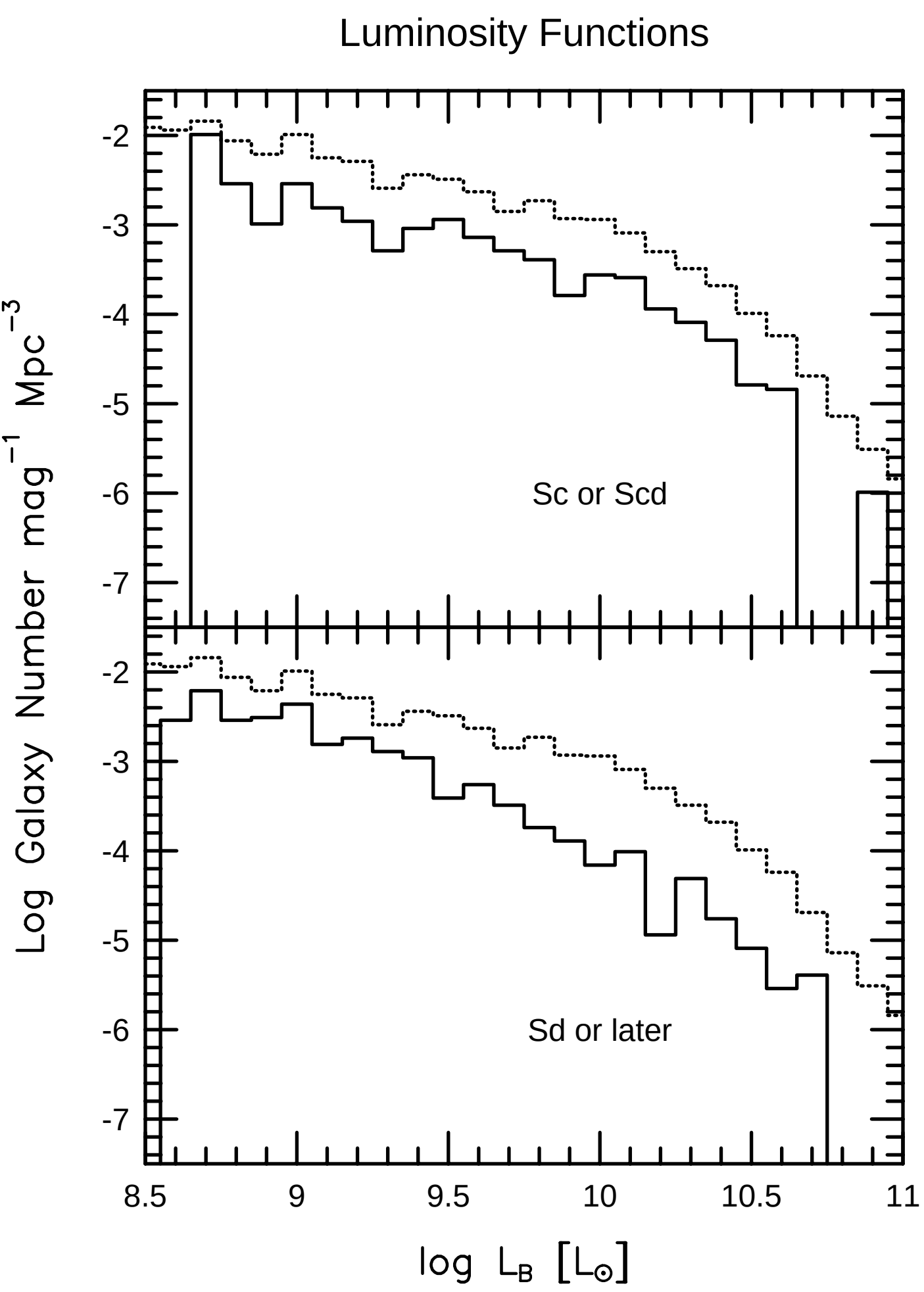
Luminosity Functions
Log Galaxy Number mag^{-1} Mpc^{-3}
-2
-3
-4
-5
-6
-7
Sc or Scd
Sd or later
8.5
9
9.5
10
10.5
11
log L_B [$L_\odot$]

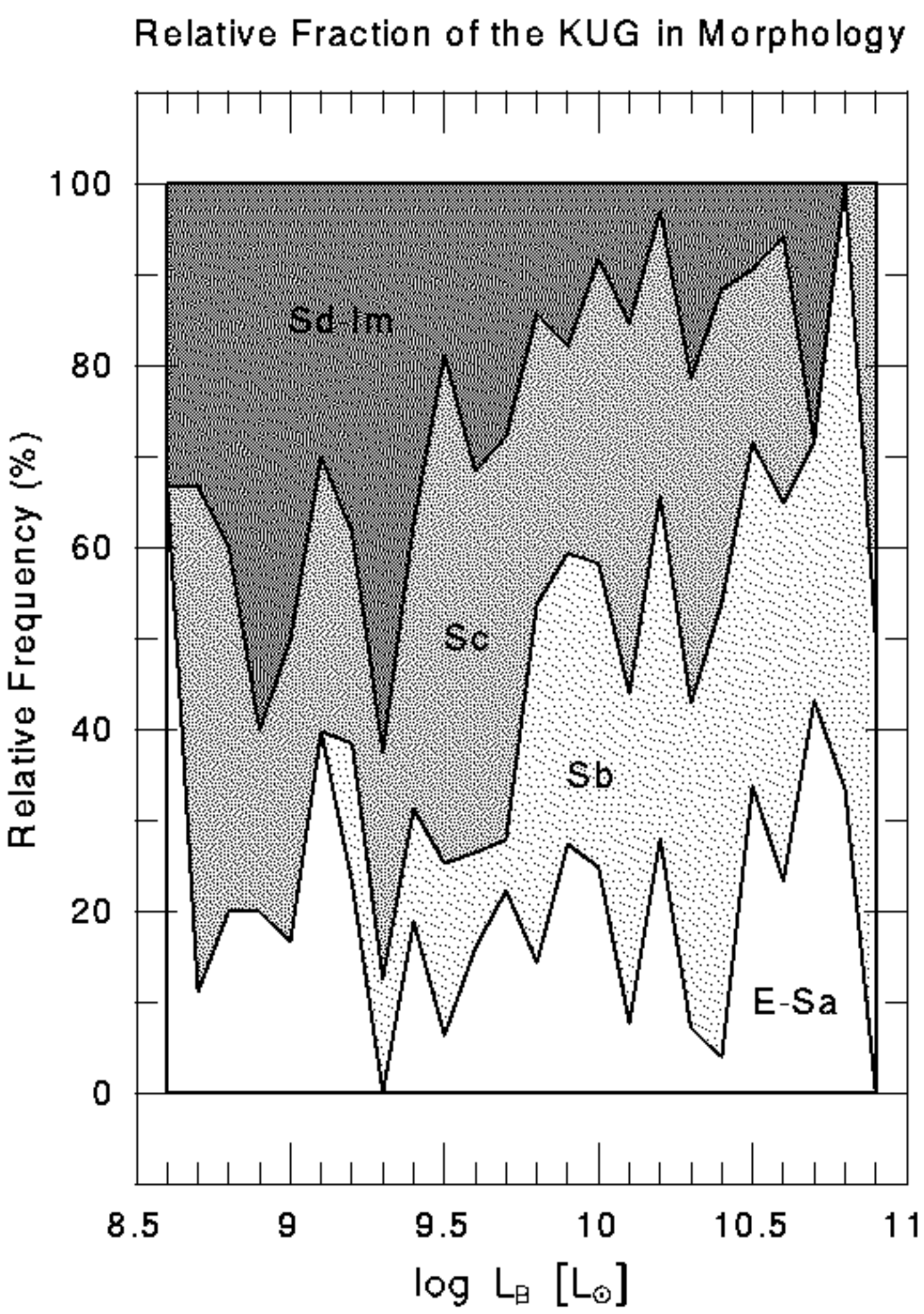
Relative Fraction of the KUG in Morphology
100
80
60
40
20
0
Relative Frequency (%)
Sd-Im
Sc
Sb
E-Sa
8.5
9
9.5
10
10.5
11
log L_B [L_⊙]

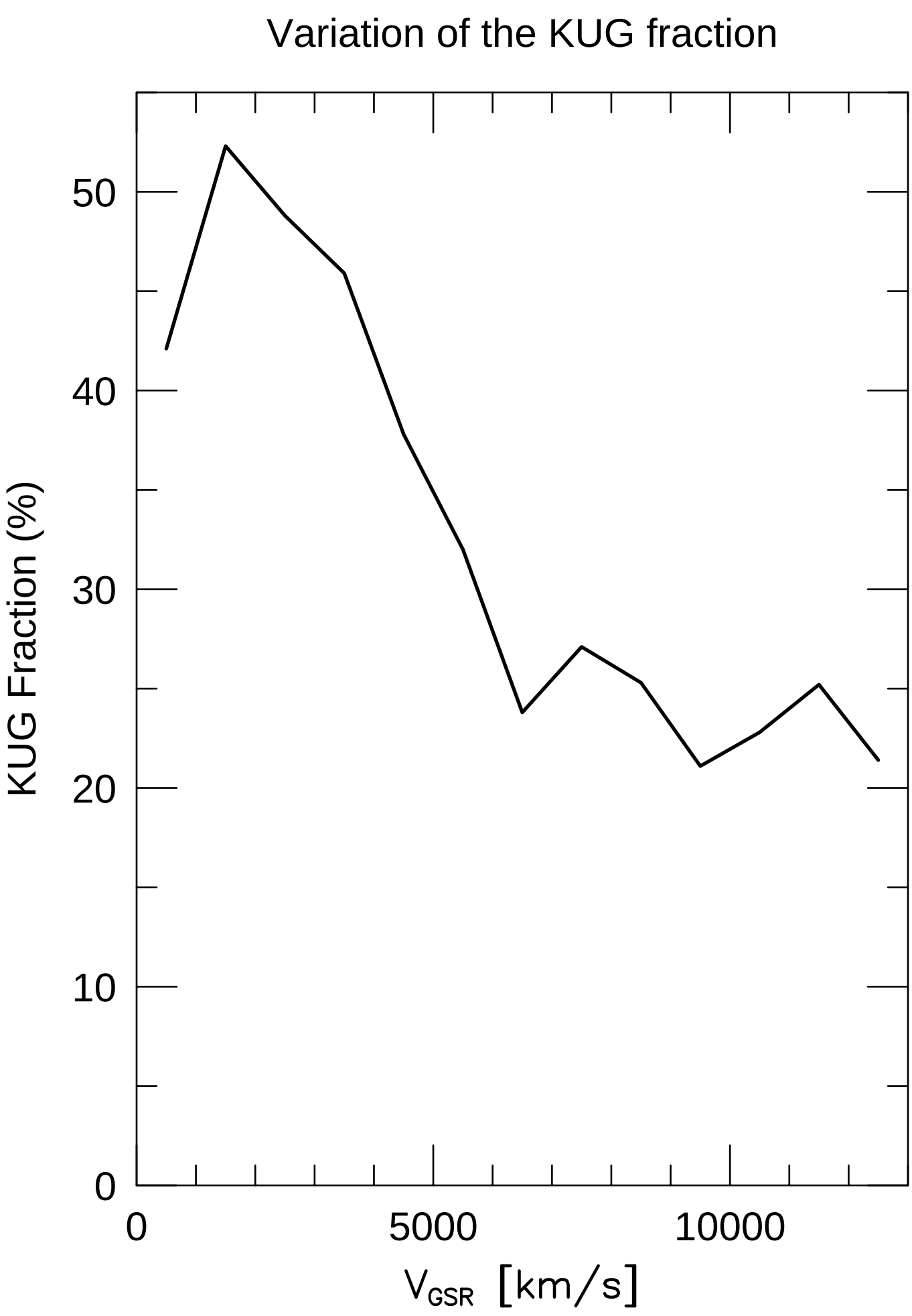
Variation of the KUG fraction
KUG Fraction (%)
0
10
20
30
40
50
0
5000
10000
V_{GSR} [km/s]

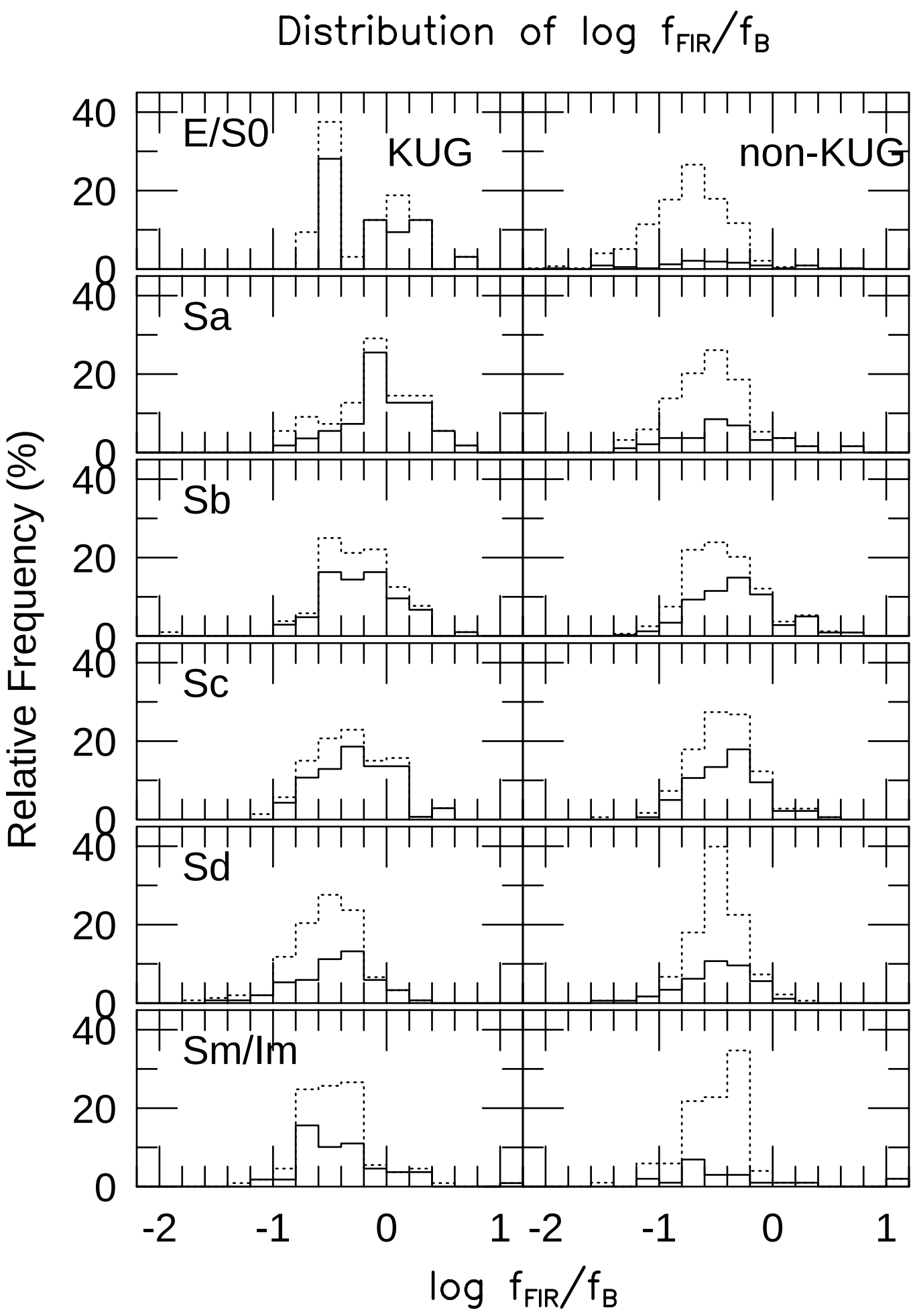
Distribution of log f_{FIR}/f_B
E/S0
KUG
non-KUG
Sa
Sb
Sc
Sd
Sm/Im
Relative Frequency (%)
0
20
40
-2
-1
0
1
log f_{FIR}/f_B